Title:

Memory-specific encoding activities of the ventral tegmental area dopamine and GABA neurons

Authors: Vasileios Glykos[1,2,*], Shigeyoshi Fujisawa[1,*]

Affiliations: [1]Laboratory for Systems Neurophysiology, RIKEN Center for Brain Science, 2-1 Hirosawa, Wako, Saitama 351-0198, Japan

[2]Present address: Synapse Biology Unit, Okinawa Institute of Science and Technology, 1919-1 Tancha, Onna-son, Kunigami-gun, Okinawa, Japan 904-0495

*Corresponding author: shigeyoshi.fujisawa@riken.jp, vasileios.glykos@oist.jp

Abstract

Although the midbrain dopamine (DA) system plays a crucial role in higher cognitive functions, including updating and maintaining short-term memory, the encoding properties of the somatic spiking activity of ventral tegmental area (VTA) DA neurons for short-term memory computations have not yet been identified. Here, we probed and analyzed the activity of optogenetically identified DA and GABA neurons while mice engaged in short-term memory-dependent behavior in a T-maze task. Single-neuron analysis revealed that significant subpopulations of DA and GABA neurons responded differently between left and right trials in the memory delay. With a series of control behavioral tasks and regression analysis tools, we show that firing rate differences are linked to short-term memory-dependent decisions and cannot be explained by reward-related processes, motivated behavior, or motor-related activities. This evidence provides novel insights into the mnemonic encoding activities of midbrain DA and GABA neurons.

KEYWORDS: Short-term memory, ventral tegmental area, dopamine, GABA

Introduction

Dopamine (DA) neurons originating in the ventral tegmental area (VTA) project to diverse forebrain regions, forming distinct but interacting neuromodulatory systems that are thought to play pivotal roles in the regulation of reward-related learning, motivation, and cognition (Sawaguchi and Goldman-Rakic, 1991; Schultz et al., 1993; Goldman-Rakic, 1995; Schultz et al., 1997; Tzschentke, 2001; Schultz, 2002; Pierce and Kumaresan, 2006; Berridge, 2007; Vijayraghavan et al., 2007; Lammel et al., 2008; Robbins and Arnsten, 2009; Hauber, 2010; Cohen et al., 2012; Salamone and Correa, 2012; Howe et al., 2013; Matsumoto and Takada, 2013; Hamid et al., 2016; Mohebi et al., 2019). A wealth of electrophysiological recordings from midbrain DA neurons, complemented by *in vivo* microdialysis data indicate that midbrain DA activity promotes behaviors associated with motivation (Wise, 2004; Berridge, 2007; Salamone and Correa, 2012; Howe et al., 2013; Matsumoto and Takada, 2013; Hamid et al., 2016; Mohebi et al., 2019) and supports reward-based learning by encoding reward prediction error (RPE) signals (Schultz et al., 1993; Schultz et al., 1997; Cohen et al., 2012).

Also, DA is of central importance to higher cognitive functions, such as updating and maintaining short-term memory (Sawaguchi and Goldman-Rakic, 1991; Miller and Cohen, 2001; Ott and Nieder, 2019). Pioneering behavioral studies which pharmacologically manipulated the activity of DA receptors in the PFC revealed the significant role of DA signals on short-term memory. In fact, an inverted-U-shape effect was discovered, where too little or too much DA receptor stimulation impairs PFC-engaging short-term memory (Sawaguchi and Goldman-Rakic, 1991; Vijayraghavan et al., 2007; Robbins and Arnsten, 2009). Moreover, at the origin of the DA system, electrophysiological recordings at the VTA showed that DA neurons are not active in the delay period of memory tasks (Ljungberg et al., 1991; Schultz, 2002; Phillips et al., 2004; Matsumoto and Takada, 2013; Choi et al., 2020).

Motivated by the response of DA neurons to reward-related stimuli and memory delays, several lines of computational modeling studies sought to answer when and how DA signals support short-term memory "update" and "maintenance". They proposed the "gating theory", which provided a unified computational framework for reward

prediction and short-term memory (Cohen et al., 2002; Dreher and Burnod, 2002; Montague et al., 2004; Ott and Nieder, 2019). According to the model, reward-predicting cues, elicit phasic DA release which opens the gate for the afferent signals to be stored in memory (update). But, in the delay period, low, tonic DA levels close the gate for interfering signals to enter the PFC and overwrite the short-term memory component (maintenance). Although the "gating theory" fits adequately the behavior-unique responses of DA neurons to the coding schemes of short-term memory, it relies mainly upon empirical evidence of the population activity of DA neurons and the longstanding consensus that short-term memory depends on the unbroken chain of persistent neuronal activity (Durstewitz et al., 2000; Curtis and D'Esposito, 2003).

However, recent advances in the study of the brain's functional organization suggest that persistent neuronal activity might not be the only candidate mechanism for the active maintenance of goal representation over short delays, leading to the proposal of new coding schemes for short-term memory (Stokes, 2015; Miller et al., 2018). One of these candidate mechanisms regards the memory-dependent dynamic changes in functional connectivity. Neural oscillations are abundant in the mammalian brain and are thought to offer the networking framework for the temporal organization of neuronal activity and information processing in short-term memory (Uhlhaas and Singer, 2006; Buschman et al., 2012; Miller et al., 2018). Calculating the phase coherence of neural oscillations between distributed brain regions provides an estimation of the functional connectivity between them (Fries, 2005). Among other basal ganglia regions, the VTA engages dynamically in the large-scale network of brain systems that support memory-related information processing. Simultaneous electrophysiological recordings were performed in the PFC and the VTA while rodents executed memory-guided behavioral choices in a T-maze task (Fujisawa and Buzsáki, 2011). Neural oscillations (4Hz) were prominent in both regions throughout the task, but their power and coherence were adaptively increased in memory delay. In the same task, another short-term memory-related coding scheme was reported, this time at the single neuronal level. It was shown that while rodents navigate the maze, performing memory-guided decisions, PFC and parietal neurons differentiate their firing activities between opposite behavioral choices (Fujisawa et al., 2008; Harvey et al., 2012). Neuronal preference for choices was

prominent in the delay period of the memory task but diminished in control non-memory behavioral tasks. To summarize, this novel empirical evidence from rodent studies on the Tmaze behavioral apparatus complements the coding framework of short-term memory with more dynamic and adaptive information-processing mechanisms other than persistent activity. Notably, by averaging neuronal population activities, none of these computational schemes would have been revealed.

In studying the role of DA neurons in short-term memory, we should take into consideration that the DA neuronal circuit is by no means self-contained and therefore it should not be investigated in isolation. Neurons utilizing GABA as a neurotransmitter constitute approximately 30% of the VTA neuronal population. The memory-related encoding properties of these inhibitory neurons have been largely overlooked, despite evidence of a strong inhibitory influence on neighboring DA neurons (Nair-Roberts et al., 2008; Omelchenko and Sesack, 2009; Tan et al., 2012; van Zessen et al., 2012) and well-established interconnections with the PFC circuit (Carr and Sesack, 2000a, b).

In light of the above, we wished to investigate with fine temporal and spatial resolution the firing activity of optogenetically identified DA and GABA neurons while mice performed a T-maze reward-seeking task with memory load. We took into consideration that (i) earlier studies analyzed either the population activity of putative DA neurons or drew inferences of the population activity from voltammetry measurements (Ljungberg et al., 1991; Schultz, 2002; Phillips et al., 2004; Matsumoto and Takada, 2013; Choi et al., 2020), and (ii) field potentials (like the 4Hz oscillations recorded in the VTA) stem mainly from phase-aligned excitatory or inhibitory post-synaptic potentials, whereas spiking activity is sparse (Traub et al., 2004; Buzsaki, 2006). (iii) A recent report revealed the causal relationship of DA activity with short-term memory, by inhibiting DA neurons with optogenetic tools. However, they did not report the encoding properties of single VTA DA neurons (Choi et al., 2020). Therefore, we looked for hints of memory-related encoding activities in single DA and GABA neurons by characterizing their firing preference for opposite behavioral choices.

120 ## Results

121 **Optogenetic identification of DA and GABA neurons in the VTA.**

122 In the present study, we sought to investigate the encoding properties of DA and GABA
123 neurons of the VTA while mice engage in memory-dependent reward-seeking behavior.
124 To identify neurons, we expressed the light-gated cation channel, channelrhodopsin-2
125 (ChR2), in DA and GABA neurons by injecting an adeno-associated virus containing
126 FLEX-ChR2 into DAT-Cre and VGAT-Cre transgenic mice, respectively (Bäckman et
127 al., 2006; Tsai et al., 2009; Vong et al., 2011) (Figure 1A). Optogenetic identification
128 and parallel electrophysiological recordings were performed using a custom-made
129 diode-probe system (diode-fiber assemblies attached to high-density silicon
130 probes(Stark et al., 2012), (Figures 1A and S1). For each neuron, we assessed the
131 response to light pulse trains delivered before and after behavioral sessions (Figures 1
132 and fig. S1 and S2). We identified 104 neurons recorded from five DAT-Cre mice
133 (hereafter referred to as DA neurons) and 74 neurons recorded from four VGAT-Cre
134 mice (GABA neurons) with significant excitatory responses to light pulses (Figure 1B).
135 Light-induced spikes from these neurons were almost identical to spontaneous spikes
136 (waveform correlation coefficient > 0.9, Figure S1E and 1F). In addition, the
137 electrophysiological profiles of the identified neuronal populations resembled those of
138 previous studies (i.e., DA neurons fired action potentials with both wider waveforms
139 and slower spontaneous firing rates than GABA neurons; Figure S1G), confirming the
140 selective expression of ChR2 in DA and GABA neurons (Cohen et al., 2012; Tan et al.,
141 2012).

142

143 **Behavioural Performance in a memory-dependent decision-making task.**

144 Mice were trained to perform sensory-guided and memory-dependent decisions in the
145 "Memory Task" (Figures 2A, S3A and S3B). This task required animals to associate a
146 visual cue presented at the beginning of the trial with a rewarded side arm of a figure-
147 eight T-maze. A short memory delay was introduced between cue presentation and

action selection. Following a correct response, they received water (5 µl) from a waterspout located at the end of each arm. Depending on the individual features of cognitive demand, the maze apparatus was divided into separate sections (i.e., "start," "cue," "delay," "side arms," and "reward"). To ensure that the mice made choices guided by the visual cues and had minimal influence from other behavioral parameters on decisions, we eliminated imbalances between the left and right trials in key task parameters (e.g., reward amount, visual environment, effort, and motor skill requirements).

At the time of neurophysiological data collection, all mice performed memory task trials with high accuracy. Averaging across sessions, the total correct rate was 86.8 ± 7.9% (mean ± standard deviation [SD]; left: 88.1 ± 10.0%, right: 87.2 ± 11.6%; paired *t*-test evaluating left vs right performance rate: $t(59) = 0.46$, $P = 0.65$, 60 sessions in nine mice, Figure 2B). In addition, performance was independent of individual preference for the left-or-right arm visits in any of the recorded sessions (test of independence, $\chi^2(1) < 3.84$, $P > 0.05$, Ho: correct rate is independent of arm choice, Figure S3C).

We also assessed the contribution of memory-related processing to task performance. To achieve this, we delivered blocks of trials with different memory loads in separate training sessions. Across all sessions, the correct performance rate dropped with higher memory load demands (mean ± SD; low load: 83.1 ± 8.3%, high load: 73.9 ± 9.5%; paired *t*-test on correct performance rate: $t(12) = 4.33$, $P < 0.001$, 13 sessions in seven mice, Figure 2C). This result is consistent with earlier reports (Floresco and Phillips, 2001; Floresco and Magyar, 2006) and highlights the important role of memory in supporting decisions in the present task.

The population activity of DA neurons is not elevated during the memory task trials.

DA neurons are not known to be active in the delay period of short-term memory tasks (Ljungberg et al., 1991; Schultz et al., 1993; Phillips et al., 2004; Matsumoto and

176 Takada, 2013; Choi et al., 2020), even though DA is a key neurotransmitter in the
177 regulation of prefrontal cortical mnemonic functions (Goldman-Rakic et al., 1989;
178 Smiley et al., 1992; Smiley and Goldman-Rakic, 1993; Goldman-Rakic, 1997;
179 Tzschentke, 2001). This well-established notion has been mainly inferred from the
180 average analysis of putative neuronal population activities and striatal voltammetry
181 recordings (Ljungberg et al., 1991; Schultz, 2002; Phillips et al., 2004; Matsumoto and
182 Takada, 2013; Choi et al., 2020). Corroborating these earlier reports, the average
183 discharge rate of identified DA neurons in the present study remained essentially
184 constant (Figure 2D). Simple linear regression analysis, with the neuronal firing rate as
185 the response variable and the animal's position on the maze as the single predictor
186 variable, showed that from the beginning until the end of the trial (a 1.5-meter distance),
187 the population activity of DA neurons deviated slightly by 0.17 ± 0.62 Hz (mean ±
188 standard error of the mean [SEM], did not differ from a distribution with a mean equal
189 to zero; one-sample *t*-test on the position coefficient, $t_{(103)} = 0.275$, $P = 0.78$). Notably,
190 in the memory-delay period, the discharge rate of DA neurons declined by - 0.72 ± 2.3
191 Hz (mean ± SEM, one-sample *t*-test on the position coefficient, $t_{(103)} = -0.31$, $P = 0.75$).
192 On the other hand, the GABA neurons elevated their discharge rate by 4.29 ± 1.10 Hz in
193 the delay period (mean ± SEM, one-sample *t*-test on the position coefficient, $t_{(73)} = 4.09$,
194 $P < 0.001$), confirming evidence from an earlier report (Cohen et al., 2012).

195

196 **DA and GABA neurons in the VTA show trajectory-specific encoding preferences**
197 **in short-term memory-dependent behaviors**

198 Making interpretations of the encoding properties of single neurons from population
199 rate averages is highly challenging in tasks with many behavioral choices, especially for
200 functionally heterogeneous populations such as the DA neurons. To overcome this
201 limitation, we analyzed the firing activity of single neurons, by taking into consideration
202 two important behavioral parameters. First, in every trial, the animals visited either the
203 left or right rewarded side arms. Therefore, we grouped and averaged trial spike trains
204 of single neurons by the corresponding lap trajectories (left or right; see also Methods
205 and Figure S4A). Also, in the present task, significant behavioral events (including

visual cue presentation, memory delay, and reward delivery) were inherently bound to fixed positions in the maze (Figure 2A, S3A and S3B). Thus, we arranged spiking events according to their position, to get an estimate of the behavioral correlates of neuronal activity. To this end, individual trial trajectories were linearized and represented as a one-dimensional vector consisting of 100 linearly spaced points (trial start: point 0; trial reward: point 100).

Examples of discharge patterns arranged by position and trajectory are shown in Figures 3A, S5A and S5B. These representative neurons differentiate their responses between left and right trials at certain maze positions in a robust manner. To assess the trajectory-specific effects on neuronal firing activity, we used the permutation method (Figure S4). First, we calculated the original difference between the average firing rates in the left and right trials. We then randomly reassigned the trajectory labels (left or right) on the trial spike trains and produced the permuted average firing rate differences. If neurons were modulated by trajectory, the original and permuted firing rate differences were significantly different. Since spiking events are arranged by position, the permutation method can also detect positions with significant differences.

Figure 3B summarizes the results from the permutation analysis applied to the populations of 104 DA and 74 GABA neurons. In the left and middle heatmaps, we organized the normalized mean firing rates for the preferred and non-preferred lap trajectories (i.e., trajectories with higher and lower firing rates respectively). The right heatmap contains the maze positions with significant firing rate differences. In both neuronal populations, there was abundant trajectory-specific activity, concentrated mostly in the delay and side-arm sections. Almost 20% of DA neurons differentiated their response between left or right trajectories in those maze sections (21% in the delay section and 22% in the side-arm section, 104 neurons, permutation test, $P < 0.05$, Figure 3B and Table S1). In GABA neurons, the percentage was even higher, with almost 50% of these cells eliciting trajectory-specific activities (47% in the delay section and 47% in the side-arm section, 74 neurons, permutation test, $P < 0.05$, Figure 3B and Table S1).

235 There have been reports of DA neurons discriminating between visual cues in a T-maze
236 task (Engelhard et al., 2019) or choice selections in delayed-match-to-sample tasks
237 (Matsumoto and Takada, 2013; Choi et al., 2020). However, in the present study, VTA
238 neurons did not exhibit different levels of activity in the cue section. Furthermore,
239 neuronal preference for trajectories was not restricted to the turning point, which could
240 indicate neuronal engagement in motor preparation for choice execution. Instead, it was
241 spread in a wider area, covering a distance from the memory delay onset until the end of
242 the side arms.

243 A plausible explanation for the trajectory-specific responses in the side arms is that
244 neurons were under the control of the sensory, motor, or goal-directed behavioral
245 processes triggered by the opposite trajectories (Howe et al., 2013; Hamid et al., 2016;
246 Mohebi et al., 2019). However, in the memory-delay section, trajectories were identical
247 for the left and right trials, which could be suggestive of the engagement of these
248 neurons in short-term memory processing. Neuronal preferences to arm visits in
249 memory delay are not uncommon in T-maze tasks. They have been reported in
250 prefrontal and post-parietal cortical neurons and have been attributed to short-term
251 memory-dependent decisions (Fujisawa et al., 2008; Harvey et al., 2012). So, is the
252 trajectory-specific activity in our task reminiscent of internally generated, memory
253 representations, or can be attributed to the well-known DA-linked neuronal
254 computations (Schultz, 2002; Cohen et al., 2012; Berke, 2018; Engelhard et al., 2019)?
255 To test this hypothesis, we proceeded to a series of statistical analyses and control
256 behavioral tasks.

257

258 **Multiple regression analysis confirms the trajectory-specific effect on DA and**
259 **GABA neurons.**

260 We discovered that significant proportions of VTA neurons fired preferentially for left
261 or right trajectories at specific locations on the maze when we arranged discharge
262 patterns by arm visit and position. This result does not attest that trajectory and position
263 alone contribute to the neuronal firing rate. Midbrain DA neurons are known to respond

264 to a wide variety of behavioral parameters (i.e., choice accuracy, reward history,
265 running speed, and distance to rewards (Engelhard et al., 2019)) which could also exert
266 a significant effect on neuronal firing activity. However, their effect could be dampened
267 due to the specific firing range arrangement.

268 Since these behavioral variables are difficult to control with behavioral tasks, we
269 assessed their contribution to neuronal responses using multiple regression analysis
270 (Figure S6 and Supplementary Text 1). We found that all the examined variables (lap
271 trajectory, trial number, speed, trial accuracy, and reward history) contributed to the
272 firing activities of neuronal subpopulations; however, only the lap trajectory predictor
273 could explain better the trajectory-specific activities observed in the ~20% of DA and
274 ~50% of GABA neurons that were identified with the permutation analysis.

275

276 **Memory-dependent but not motivated behavior is related to trajectory-specific**
277 **activity in VTA neurons**

278 Next, we investigated the contribution of short-term memory in decision-making on the
279 trajectory-specific activity of VTA neurons. Memory-dependent decision-making
280 depends on three major computational components. These are (i) sensory input gating,
281 (ii) maintaining and manipulating memory contents and (iii) generating and executing
282 appropriate motor plans (Cohen et al., 2002; Dreher and Burnod, 2002; Montague et al.,
283 2004; Ott and Nieder, 2019).

284 We eliminated all three components in a variation of the memory task. Specifically, we
285 trained mice in the no-cue-no-choice task, in which they were not presented with a
286 visual cue and, therefore, could not make predictions about the location of the reward
287 (Figures 4A, S3A and S3B). Furthermore, the choice selection was prevented by the
288 presence of blocked side arms when they arrived at the T-intersection. After a short
289 delay (approximately 1 s), access to one of the side arms (chosen pseudo-randomly) was
290 permitted, which always led to a reward.

291 In recording sessions, mice received mixed protocols composed of randomly interleaved
292 memory task and no-cue-no-choice task trials. We evaluated the trajectory-specific
293 activities on each task separately using the permutation method. In the delay section of
294 the no-cue-no-choice task, we observed a significant reduction in the number of
295 positions with a significant firing rate difference (mean ± SD; DA: memory task 5.9 ±
296 3.8 points, no-cue-no-choice task 1.5 ± 3.4 points, paired *t*-test, $P = 0.002$, four animals;
297 GABA: memory task 10.7 ± 3.9 points, no-cue-no-choice task 1.5 ± 2.0 points, paired *t*-
298 test, $P < 0.001$, three animals, Figures 4B to 4E). The attenuating effect on trajectory-
299 specific activity was also reflected by a marked reduction in the number of trajectory-
300 specific neurons (Figure 4E, numbers in parentheses). However, the firing rate
301 difference between the left and right-side arms was strong in both tasks (DA: memory
302 task 8.5 ± 7.8 points, no-cue-no-choice task 5.9 ± 7.4 points, paired *t*-test, $P = 0.139$,
303 four animals; GABA: memory task 12.6 ± 8.1 points, no-cue-no-choice task 9.9 ± 8.8
304 points, paired *t*-test, $P = 0.234$, three animals, Figures 4B to 4E).

305 However, the significant reduction in trajectory-specific encoding preference in the no-
306 cue-no-choice task could not be entirely attributed to the absence of the memory
307 component. This is because important running speed, motor responses, and motivational
308 discrepancies exist between memory and no-cue-no-choice tasks. With regard to
309 motivation, the important role of DA in adaptive decision-making is widely recognized
310 (Hamid et al., 2016; Berke, 2018; Mohebi et al., 2019). We did not observe animal
311 choice bias in memory task performance (Figures 2B and S3C), but we cannot rule out
312 the possibility that individual neurons were modulated differently by effortful actions to
313 reach the left- and right-sided rewards (Figure S7). Unlike the memory task, in the no-
314 cue-no-choice task, the mice could not direct behavior towards the left- or right-side
315 arms due to the absence of a visual cue. As a result, they were unable to allocate
316 incentive motivational drives to the left-or-right trials (Howe et al., 2013; Hamid et al.,
317 2016; Berke, 2018; Mohebi et al., 2019). Also, the initial access denial to the side arms
318 in the control task eliminates any potential differences in the motor preparation coding
319 schemes (according to the "gating theory") for the opposite arm visits in the memory
320 task (Engelhard et al., 2019; Ott and Nieder, 2019). Finally, regarding speed, a

representative example of running speed differences between the two tasks within a single session is shown in Figure 4F.

To dissociate the short-term memory component of neuronal activity from the modulatory effects of running speed, incentive motivation, and motor-related signaling, we trained mice in a second control task. The cue-no-choice task preserved the same running speed parameters (Figure S8), motor skill requirements, and physical effort demands (i.e., visual cues, maze shape, arm length, and reward amount were the same) as the memory task, but it prevented animals from making decisions. Accordingly, the animals were presented with the same visual cue as in the memory task, which indicated the side arm that was rewarded and enabled them to allocate incentive motivational drive to the left-or-right trials; however, they were always forced to visit the rewarded arm by blocked access to the unrewarded arm (Figures 5A, S3A and S3B). In the same recording session, the mice performed a separate block of memory task trials. Similar to the first control task, in the delay section of the cue-no-choice task we observed a significant reduction in the spatial extent of the firing rate difference (DA: memory task 5.4 ± 3.6 points, cue-no-choice task: 0.4 ± 1.1, paired *t*-test, $P = 0.011$, four animals; GABA: memory task 10.7 ± 6.3 points, cue-no-choice task 3.5 ± 4.2 points, paired *t*-test, $P < 0.001$, 1 animal, Figures 5B to 5E). In the side arms, however, the trajectory-specific effect remained strong and was not significantly different from the effect observed in the memory task (DA: memory task 8.1 ± 10.3 points, cue-no-choice task 5.0 ± 4.6 points, paired *t*-test, $P = 0.146$, four animals; GABA: memory task 8.7 ± 5.9 points, cue-no-choice 5.2 ± 6.2 points, paired *t*-test, $P = 0.086$, 1 animal, Figures 5B to 5E).

Together, these results suggest that trajectory-specific responses in the delay period of the memory task could reflect short-term memory representations linked to decision-making behavior and cannot be explained by running speed, motor, and motivation-related signaling differences.

Neuronal activities in delay and reward are unrelated

It is widely recognized that DA and GABA neurons of the VTA respond to reward and reward-predicting cues (Schultz et al., 1993; Schultz et al., 1997; Cohen et al., 2012; Matsumoto and Takada, 2013; Engelhard et al., 2019; Choi et al., 2020). Therefore, we examined whether the selective neuronal responses to left-or-right trials in the memory delay and side-arm sections could be attributed to encoding biases related to rewards. We defined the first second of reward consumption as the reward section.
DA neurons are known to be excited by rewards (Schultz et al., 1993; Schultz et al., 1997; Cohen et al., 2012; Matsumoto and Takada, 2013; Engelhard et al., 2019; Choi et al., 2020). In agreement with this notion, we discovered that 27 DA neurons (28% of 104 neurons, Figure 6B column 4) responded to reward with significant excitation, which is a high proportion considering the low uncertainty of the task due to the high-performance rate and overtraining.

We subsequently examined whether VTA neurons could discriminate between left- and right-arm rewards. DA neurons are known to discriminate between rewards with different magnitudes and predictabilities(Tobler et al., 2005; Morris et al., 2006). The animals were offered equivalent options in terms of reward magnitude, uncertainty, and effort. Thus, we predicted the presence of a small number of reward-discriminating neurons. However, we found that 23% of DA neurons and 46% of GABA neurons differed significantly in their responses to left-or-right rewards (Figures 6A, 6B column 3, and Table S1; paired *t*-test comparing mean firing rates, $P < 0.05$). Therefore, we assessed the relationship between encoding preferences in the reward section and those in the remainder of the maze by correlating the average firing rate difference in the reward section with the average rate difference in the preceding maze sections. In both neuronal populations, we found a significant positive relationship between the reward and side-arm sections (Figure 6C; Pearson's correlation; DA: $R = 0.31$, $P < 0.001$; GABA: $R = 0.67$, $P < 0.001$) but not between the reward and delay sections (Figure 6C; Pearson's correlation; DA: $R = -0.05$, $P > 0.05$; GABA: $R = -0.03$, $P > 0.05$). These results demonstrate that trajectory-specific firing activities in memory delay do not reflect reward preference during consumption.

380 ## Discussion

381 In the present study, we performed extracellular recordings from optogenetically
382 identified DA and GABA neurons in the VTA while mice performed reward-seeking
383 tasks on a T-maze apparatus. Mice were trained to choose between two spatially
384 separate goals under the instruction of visual cues presented at the beginning of the
385 trials. A short memory delay was introduced between cue presentation and choice
386 selection. We discovered that subpopulations of DA and GABA neurons showed
387 differential responses between the left and right trials, starting from the onset of the
388 memory delay period in the main arm, where the trajectories were indistinguishable.
389 Trajectory-specific preference was not correlated with reward history, running speed,
390 the incentive motivational drive of physical effort, or reward-related encoding
391 differences, and diminished significantly when the memory-dependent decision
392 component was eliminated in control behavioral tasks. This evidence indicates that
393 populations of DA and GABA neurons in the VTA encode internally generated signals
394 that support short-term memory in decision-making.

395

396 **Activities of midbrain DA neurons in short-term memory**

397 The well-established notion that DA somatic spiking activity is low in short-term
398 memory stemmed mainly from firing rate averages of putative neuronal populations
399 (Ljungberg et al., 1991; Schultz, 2002; Phillips et al., 2004; Matsumoto and Takada,
400 2013; Choi et al., 2020). Consistent with those reports we did not observe a profound
401 variation in the population activity of DA neurons during the memory task. However, a
402 wealth of recent studies has shown that DA neurons are functionally and genetically
403 segregated (Lammel et al., 2008; Lammel et al., 2011; Engelhard et al., 2019).
404 Moreover, in many real-life situations, animals have to choose between many options
405 for behavioral responses. In such behavioral conditions, averaging firing rates cannot
406 reveal the fine computational processes of single neurons. To address this limitation, we
407 analyzed the firing activities of identified single neurons, focusing on different
408 discharge patterns between behavioral choices. Here, we demonstrated that memory-

409 specific activities by midbrain DA neurons can be represented as trajectory-specific
410 responses in the delay period of the memory task.

411 The "gating theory" unifies the signaling activities of DA neurons in reward prediction
412 and short-term memory (Cohen et al., 2002; Dreher and Burnod, 2002; Montague et al.,
413 2004; Ott and Nieder, 2019). Our evidence does not question the validity of this
414 computational model, since we do not provide evidence of how the selective preference
415 for one response over the other translates into the release site. However, it is worth
416 noting that trajectory-specific activities we observed here were rare in the visual-cue
417 section when the updating of sensory information takes place. Moreover, firing rate
418 differences between left and right-arm responses declined in a control behavioral task
419 (cue-no-choice) without memory load, but with the same motor skill requirements as the
420 memory task. Thus, motor preparation coding schemes for different responses (Cohen et
421 al., 2002; Ott and Nieder, 2019) cannot be accounted for the trajectory-specific
422 activities in the memory delay. Instead, our evidence indicates that trajectory-specific
423 activities by DA (also GABA) neurons are functionally linked to the maintaining and
424 manipulating of memory contents.

425 Memory-related, trajectory-specific neuronal activities have also been reported for PFC
426 and post-parietal neurons while rodents perform reward-seeking responses on the T-
427 maze (Fujisawa et al., 2008; Harvey et al., 2012). Furthermore, in the same task, both
428 the PFC and VTA circuits are functionally engaged with coherent 4-Hz oscillations in
429 the memory delay (Fujisawa and Buzsáki, 2011). Our results complement this line of
430 work, demonstrating that also DA and GABA midbrain neurons elicit memory-related,
431 trajectory-specific activities.

432 The present study also corroborates important findings from a recent report, which
433 demonstrated that optogenetic perturbations in DA neuron excitability exert a strong
434 effect on short-term memory performance, highlighting the causal role of DA neuronal
435 firing activity in memory-dependent behavior (Choi et al., 2020). Also, in agreement
436 with a previous report (Engelhard et al., 2019) by the same laboratory, we show that
437 subpopulations of VTA neurons are modulated by running speed, cumulative
438 performance rate, current choice accuracy, and reward history. Disparities between this

439 and our study in the proportions of modulated neurons could be attributed to the
440 different recording techniques applied as well as the maze regions of interest; for
441 example, Engelhard et al. analyzed neuronal firing activities in the visual-cue period
442 (Engelhard et al., 2019), whereas we focused on memory delay.

443 Overall, our results are in agreement with the notion that DA neurons encode a variety
444 of behavioral parameters in complex environments. In addition, we confirmed that in
445 memory-dependent behaviors, DA neuronal populations did not elicit sustained
446 increases in their discharge rate. However, in the present task, DA neurons individually
447 encoded internal representations by differentiating their responses to lap trajectories in
448 memory delay.

449

450 **Role of motivated behavior in trajectory-specific encoding properties of VTA**
451 **neurons**

452 Midbrain DA activity is known to be involved in motivated behavior while rodents
453 navigate mazes to receive rewards in trials lasting a few seconds (Hamid et al., 2016;
454 Berke, 2018; Mohebi et al., 2019). When mice approach rewards, striatal DA
455 concentrations increase, scaling flexibly with reward size and proximity, which is
456 proposed to reflect a neural correlate of a sustained motivational drive (Howe et al.,
457 2013). To evaluate the role of motivated behavior in the trajectory-specific preference
458 of midbrain neurons, we compared firing activities between a memory task and a
459 control task without memory-dependent decisions (cue-no-choice task). Although in the
460 cue-no-choice task, the behavioral parameters that determined the incentive
461 motivational drives were the same as in the memory task (visual cues, maze shape, and
462 reward amount), neuronal responses did not differ between the left and right trials. This
463 result strongly indicates that incentive motivational drives (at least for physical effort)
464 do not contribute to trajectory-specific activities of midbrain neurons during the delay
465 period of the memory task.

466

467 **Memory-specific activities of the VTA neurons are not attributed to reward**
468 **prediction error signaling**

469 We also assessed the role of reward-related processing in the trajectory-specific activity
470 of the midbrain neurons. In behavioral tasks in which animals estimate the spatial
471 proximity of distant rewards, it has been suggested that DA neurons calculate RPE
472 signals from state-value functions (Hamid et al., 2016; Berke, 2018; Engelhard et al.,
473 2019; Mohebi et al., 2019; Kim et al., 2020). In the present study, the animals received
474 ongoing visual input, facilitating the continuous estimation of reward proximity. Thus,
475 DA neurons can potentially estimate RPE signals from successive state values assigned
476 to each position on the maze track (Figure S7). Therefore, the difference in firing
477 activity between the left and right trials could be the result of differences in the state-
478 value functions assigned to these trajectories (Hamid et al., 2016; Berke, 2018).
479 However, significant evidence contradicts this hypothesis.

480 First, the behavioral parameters that determine the state-value functions for the left and
481 right trajectories were set to be identical in the cue-no-choice task and memory task, by
482 preserving the same maze configurations and delivering equal amounts of reward. In
483 addition, behavior in both tasks was cue-driven; therefore, animals could make
484 predictions about the reward location and orchestrate behavior accordingly. However,
485 we observed a prominent reduction in the firing rate difference between the left and
486 right trials in the cue-no-choice task (Figure 5). Second, a significant subset of DA
487 neurons (approximately 20%) responded differently to the left and right rewards in the
488 memory task, although the same amount of reward was delivered. This unexpected
489 finding raised the hypothesis that the encoding preference for reward could be reflected
490 in the values of the preceding states in the maze and, therefore, could account for the
491 trajectory-specific effect in memory delay. However, the differences in the firing
492 activity elicited by the consumption of left-or-right rewards were unrelated to the firing
493 rate difference in the delay section (Figure 6C). In conclusion, these findings indicate
494 that the encoding preference for lap trajectories exhibited by midbrain DA and GABA
495 neurons cannot be simply explained by discrepancies in RPE signaling.
496

497 **GABA neurons of the VTA and short-term memory**

498 With the advent of highly selective identification and perturbation techniques, new
499 evidence has emerged regarding the encoding properties and functional roles of local
500 VTA inhibitory networks in reward processing and motivation. There are reports
501 demonstrating that GABA neurons of the VTA suppress reward consummatory
502 behavior (van Zessen et al., 2012), facilitate aversive behavior (Matsumoto and
503 Hikosaka, 2007; Tan et al., 2012), and elicit sustained activities in the delay period
504 between conditioned and unconditioned stimuli (Cohen et al., 2012). During these
505 behaviors, the responses of DA and GABA neurons are often inverse, such that when
506 GABA neurons are excited, neighboring DA neurons decrease their discharge rate. In
507 particular, aversive stimuli excite GABA neurons, which then suppress the neighboring
508 DA neurons (Tan et al., 2012). In addition, during reward consumption, GABA neurons
509 are inactive (Cohen et al., 2012; van Zessen et al., 2012); however, when excited, they
510 inhibit DA neurons and disturb consummatory behavior (van Zessen et al., 2012).
511 Finally, in classical conditioning tasks, DA neurons respond to rewards and reward-
512 predicting stimuli, whereas GABA neurons remain silent during such events (Cohen et
513 al., 2012). However, we demonstrated here that midbrain DA and GABA neurons elicit
514 remarkably similar encoding properties. Both neuronal populations respond to short-
515 term memory-specific activities manifested by encoding preferences for lap trajectories.
516 Notably though, GABA neurons are more strongly engaged in this dynamic encoding
517 activity since almost twice as many inhibitory neurons responded differently to the left
518 and right trials.

519 This result presents an activity paradox. Given the abundant and potent synaptic
520 inhibition of DA neurons by neighboring GABA neurons (Omelchenko and Sesack,
521 2009), it was unexpected that both populations were highly active and similarly engaged
522 in tasks. However, anatomical evidence provides a plausible explanation. Local
523 inhibitory neurons form a dense network of local synaptic innervations that target the
524 dendritic sites of DA and other GABA neurons (Traub et al., 2004; Buzsaki, 2006;
525 Omelchenko and Sesack, 2009). Although potent and well-suited for coordinated
526 network activity, this synaptic inhibition is not as strong as somatic inhibition (Jhou et
527 al., 2009; Omelchenko and Sesack, 2009), and it has been suggested that it is not

sufficient to suppress DA neurons when they receive a strong excitatory drive from extrinsic sources (van Zessen et al., 2012).

Conclusion

In summary, we optogenetically probed DA and GABA neurons in the VTA while mice performed a decision-making task with memory load. We discovered that both of these neuronal populations elicited memory-dependent preferences for left-or-right trajectories that could not be explained by motor activity, motivated behavior, or reward-related processes. This evidence indicates that VTA neurons encode mental representations to support short-term memory-dependent decisions and provides insights into novel sophisticated coding strategies employed by the midbrain DA and GABA neurons in reward-related behavior.

553 ## Methods & Materials
554

555 **Key resources table**

REAGENT or RESOURCE	SOURCE	IDENTIFIER
Antibodies		
Anti-Tyrosine Hydroxylase	EMD Millipore	
Anti-GFP	Aves Labs	
Alexa Fluor 546 IgG	Thermo Fisher Scientific	
Alexa Fluor 488 IgG	Jackson Immunoresearch Laboratories, Inc.	
DAPI Fluoromount-G	SouthernBiotech	
Bacterial and virus strains		
AAV5-EF1a-DIO-hChR2(H134R)-EYFP-WPRE-pA	UNC Vector Core	N/A
Experimental models: Organisms/strains		
Mouse: C57BL/6J-Slc6a3$^{tm1.1(cre)Bkmn/J}$	The Jackson Laboratory	Jax #006660; RRID: IMSR_JAX:006660
Mouse: C57BL/6J- Slc32a1$^{tm2(cre)Lowl}$	The Jackson Laboratory	Jax #0016962; RRID: IMSR_JAX:0016962
Software and algorithms		
MATLAB	MathWorks	https://www.mathworks.com/
KlustaKwik2	(Kadir et al., 2014)	https://github.com/kwikteam/klustakwik2
RPvdsEX	Tucker-Davis Technologies	https://www.tdt.com/component/rpvdsex/
Other		
Silicon probe: 64-site, 6-shank	NeuroNexus	Buzsaki64spL

Optical fiber AFS50/125Y	Thorlabs, Inc.	https://www.thorlabs.co.jp/thorproduct.cfm?partnumber=AFS50/125Y
Blue laser diode	OSRAM Opto Semiconductors	PL450B
256-channel Multiplexed Biosignal Amplifier	Amplipex, Ltd.	KJE-1001
Figure-eight T-maze apparatus	O'Hara & Co., Ltd.	http://ohara-time.co.jp/

CONTACT FOR REAGENT AND RESOURCE SHARING

Further information and requests for resources and reagents should be directed to and will be fulfilled by the Lead Contact, Dr. Shigeyoshi Fujisawa (shigeyoshi.fujisawa@riken.jp).

Animals

All experiments were approved by the RIKEN Institutional Animal Care and Use Committee. We used five adult male DAT-ires-Cre (Jackson's Lab; stock #6660; (Bäckman et al., 2006) and four Vgat-ires-Cre (Jackson's Lab; stock #16962; (Vong et al., 2011) mice backcrossed to C57BL/6J. Animals were housed in separate cages on a 12-h dark/light cycle and each performed the behavioral tasks at the same time of the day, between 11:00 and 17:00. In the cage, they were provided *ad libitum* food access but were restrained from water availability.

Behavioral tasks

All behavioral tasks took place on a T-maze apparatus. More information about the maze configuration is provided in Figure S3.

Memory task. Behavioral sessions commenced with the animal being placed at the "starting position" (Figures 2A, S3A and S3B). Then, access to the main corridor was

provided and the animal had to run through the “start” section (0-50 cm) before it arrived at the maze segment surrounded by two PC monitors (“visual-cue” section, 50-80 cm). In this section, it was presented with a distinctive visual object (vertical black and gray bars) in one of the two monitors (the other monitor remained dark) indicates which side arm to visit to obtain the reward (i.e., left cue → left reward, right cue → right reward). In the third region of the central arm (“delay” section, 80-120 cm) both monitors turned dark. While running in the delay section, the animal had to maintain the reward-related information and based on that perform the action selection at the T-intersection. The intersection at the end of the main arm designated the end of the delay section and the beginning of the “side-arms” section (120-150 cm) where the animal runs towards the reward position in anticipation of the reward. Reward (5 µl water) was delivered on correct trials at the end of the side-arms section from a waterspout. The first activation of the light-beam sensor at the waterspout triggered the water-delivery pump (Burkert, Ingelfingen, Germany), followed by reward consumption (“reward” section). After consuming the reward, the animal could return of its own will to the starting position, to commence a new trial.

Daily behavioral sessions consisted of 80-100 trials. Only animals with at least three successive sessions with an 80% performance ratio or more in the training phase were been proceeded to surgical operations.

No-Cue-No-Choice task. Trials of this control task were delivered in recording sessions, interleaved with memory task trials. When the animal entered the visual-cue section it was not instructed by the visual cue (Figures 4A, S3A and S3B). Also, access to both side arms was initially denied by closed sliding doors. Approximately 1 s after the animal arrived at the turning point, one of the sliding doors opened (pseudo-randomly) providing access to the reward. On every trial, the presentation or absence of the visual cue could instruct the animal about the task rules (i.e., memory task or no-cue-no-choice task).

606 ***Cue-No-Choice-task.*** The settings of this control task were the same as the memory
607 task settings, except for the blockade of the unrewarded side arm (Figures 5A, S3A and
608 S3B). Thus, the animals were always forced to perform correct choices. Because in both
609 tasks, the same cue was presented, the animals could potentially be confused about the
610 trial's task rules. Therefore, memory task and cue-no-choice task trials were delivered in
611 separate sets within the same recording session. Accordingly, when the animals
612 completed the set of cue-no-choice task trials (approximately 50 trials), they were
613 automatically delivered with another set of memory task trials (approximately 50 trials).

614 Recording sessions lasted approximately 20-30 minutes.

615

616 **Intracranial surgeries and electrophysiological recording**

617 The surgical process consisted of two separate operations. First, mice (DAT-ires-Cre or
618 Vgat-ires-Cre) were surgically injected with 200-500 nl of adeno-associated virus
619 AAV5-EF1a-DIO-hChR2(H134R)-EYFP-WPRE-pA (University of North Carolina
620 vector core facility; (Tsai et al., 2009) into the VTA stereotaxically (from inferior
621 cerebral vein AP: ~6.65 mm, from midline ML: - 0.55 mm on the left hemisphere, from
622 surface 4-4.5 mm, Figure 1A). Ten to fifteen days later, mice were implanted with a
623 silicon probe in the same AP and ML coordinates (vertical insertion was intended, 0
624 degrees; Figures 1A, S1A to S1D). We used Buzsaki64spL (NeuroNexus, Ann Arbor,
625 MI, USA) silicon probes which are composed of 6 shanks (10 mm long, 15 µm thick,
626 200 µm shank separation) and each shank has 10 recording sites (160 μm^2 each site 0.6-
627 1.0 MΩ impedance). The silicon probe was attached to a custom-made
628 micromanipulator and moved gradually to the desired depth position. On every probe
629 shank, optic fibers were firmly attached to secure an accurate and firm insertion of the
630 recording channels in the deep midbrain area (Figure S1B). For experiments where light
631 delivery was required, two of the optic fibers (shanks 2 and 5) were coupled with blue
632 (450 nm) laser diodes (PL450B, OSRAM Opto Semiconductors). Light dispersion
633 could potentially cover the axial and transverse span of all 64 channels (Stark et al.,
634 2012).

635 During recording sessions, the wide-band neurophysiological signals were acquired
636 continuously at 20 kHz on 256-channel Amplipex systems (KJE-1001, Amplipex Ltd,
637 Hungary; (Berényi et al., 2014)). Following surgery, the probe was inserted 45 μm
638 deeper in intoe brain on a daily basis, until it reached the VTA. Thereafter, the probe
639 was moved deeper by 20 μm / day. The average recording coordinates for the DAT-Cre
640 animals are 3.32 ± 0.32 mm (mean ± standard deviation) rostrocaudal and 0.82 ± 0.17
641 mm mediolateral, and for the VGAT-Cre animals, 3.52 ± 0.29 mm rostrocaudal and
642 0.90 ± 0.17 mm mediolateral (Figure S1A).
643 We cannot exclude the possibility that some neurons were recorded in successive
644 sessions because clustering analysis was performed on individual sessions.
645

646 **Data analysis**

647 Unless otherwise stated, data analysis was performed with custom-made programs
648 designed in MATLAB with Signal-processing and Statistics toolboxes.

649

650 ***Light-stimulation protocols for optogenetic identification.*** Light stimulation protocols
651 were delivered before and after the behavioral tasks. They were composed of 1, 2, 3,
652 and 4 mW blocks of 450 nm light pulses. Each block consisted of 150 square pulses (12
653 ms pulse duration; 0-1 ms and 11-12 ms contained artifacts) delivered at 1, 2, 3 to 10
654 Hz. Electrophysiological data recorded during light stimulation and behavioral
655 protocols within a single session were merged and clustered together.

656

657 ***Statistical analysis for detection of light-responsive units.*** Neurons with light-induced
658 responses exceeding the average spontaneous activity were classed as light-responsive.
659 To identify light-responsive neurons we applied the statistical analysis described in
660 detail in Figure S2.

661

Estimation of firing activity during behaviour. To estimate the neuronal firing activity while animals performed the behavioural task, we took into consideration the primary goal of this study; that is to look for trajectory-specific encoding properties, as well as the inherent limitation of the task; that is the experimenter could not control the temporal precision of the behavioural events. To overcome this limitation, we arranged firing activity by the animal's position on the maze. To do so, first, we linearized the trial trajectories and assigned them with a lap trajectory label (left or right). Then, the linearized products were divided into 100 position points and normalized so that position 0 corresponded to the starting point of the trial and position 1 to the waterspout. Second, we constructed post-distance histograms, analogous to the peri-stimulus-time-histograms (PSTHs), although the time of spiking events was replaced by the position they occurred (for the purpose of simplicity, also by habit, we will call the post-distance histograms as PSTHs). To construct accurate PSTHs we considered the exact position the spikes were discharged and the time the animal occupied this certain position. Let $n^{(k)}(x)$ be the number of spikes of a single neuron and $t^{(k)}(x)$ be the occupation time in the x_{th} position point of the k_{th} trial (Figure S4A). Then, $\hat{\lambda}(x) = \frac{1}{K} * \sum_{k=1}^{K}[n^{(k)}(x) \,/\, t^{(k)}(x)]$ where K is the number of trials, represents the average firing rate probability (spikes / sec) at position point x. To examine the trajectory-specific encoding properties of VTA neurons we produced average firing rate histograms for correct left and right trials, separately. Then, both histograms were smoothed with a Gaussian Kernel function (σ= 0.5, length of 20 position points).

Firing rate heatmap construction. To construct the normalized firing rate heatmaps shown in Figures 3B, 4C, 4D, 5C, 5D, 6B, S5C to S5E and S6B we took the following steps. First, for every neuron we produced the average firing rate for left and right correct trials. Second, we normalized both rates by dividing them with the maximum firing rate of the strongest trajectory response (e.g., for the example shown in Figure S4A we divided both average firing rates by the maximum rate of the response to the left trials). Then, the normalized rate of the stronger trajectory response was assigned to the "preferred" heatmap and the rate of the weaker trajectory response to the "non-

preferred" heatmap (e.g., for the example shown in Figure S4A, the left normalized rate was assigned to the "preferred" heatmap and the right rate to the "non-preferred" heatmap). Both rates occupied the same row. The row ordering was determined by the position of maximum rate.

Identifying trajectory-specific neurons with the permutation method. To identify neurons with trajectory-specific encoding properties we applied the permutation test reported elsewhere (Fujisawa et al., 2008) and described in detail in Figure S4.

Regression analysis. We designed a generalized linear regression model (GLM) with the neuronal firing rate (FR) modelled as a gaussian function of the lap trajectory (T), speed (S), trial number (TN), performance (R), current trial accuracy (A_0) and previous trial accuracy (A_{-1}) behavioural variables. With the permutation analysis we observed that the trajectory-specific effect on the firing activity was dependent on position. Thus, we examined the joint effect of trajectory with position (P) on spiking activity. All dependent and independent variables were arranged by position. The values of the trajectory (1 for left and 2 for right), trial number, performance (cumulative correct rate), current trial and previous trial accuracy (1 for correct trial, 0 for error trial) variables remained constant throughout the whole trial. The firing rate, position and speed variables changed their values on every position.
The GLM was:

$$FR = \beta_0 + \sum_{k=1}^{6} \beta_{T*P} T \cdot P^k + \sum_{k=1}^{6} \beta_S \cdot S^k + \beta_{TN} \cdot TN + \beta_R \cdot R + \beta_{A_0} \cdot A_0 + \beta_{A_{-1}} \cdot A_{-1} + \varepsilon$$

where the β values are the regressor coefficients for the different predictors (including the intercept β_0) and ε is the Gaussian noise term. The 6th degree order polynomials of position and speed were chosen for model optimization with the Bayes information criterion.

First, we generated model predictions of the average firing rates for left ($\hat{L}_0$) and right ($\hat{R}_0$) trials, and from those we calculated the predicted firing rate difference ($\hat{D}_0$). Then,

we shuffled the trajectory labels assigned to the tested variable (the assigned labels to the rest of the independent variables remained intact) and assessed the effect on the firing rate difference. For every predictor we produced 500 shuffled rate differences, $\widehat{D}_j$. If the absolute mean value of $\widehat{D}_0$ exceeded the top 5% of the $\widehat{D}_j$ values (including Bonferroni correction), then the hypothesis was rejected, and the predictor was significantly contributing to the firing rate difference. We examined every maze region individually, but, here we report only for the delay region.

Reward-related excitation or inhibition. The reward section was defined as the first second of reward consumption. To assess neuronal response to reward consumption and categorize it as excitatory, inhibitory or non-responsive we performed the following analysis. First, we produced the smoothed mean firing rate response in the time domain (as we did in the maze sections in the space domain) for left, $\hat{\lambda}_{Left}(t)$, and right, $\hat{\lambda}_{Right}(t)$ trials. For the preferred arm of each neuron, we compared the mean firing rate in the reward section to the mean rate in the 100 ms epoch preceding reward delivery (paired t-test on mean firing rates; $P < 0.05$; Figure 6B column 4).

Encoding preferences in the reward section. The difference in the intensity of neuronal firing activity between left and right rewards was assessed by comparing the mean firing rate of neuronal activity elicited in the reward section of left and right trials (paired t-test on mean firing rates; $P < 0.05$; Figure 6B column 3).

Relationship of encoding preferences in the reward section to those in the remainder of the maze. To assess whether the trajectory-specific firing activity in the maze was linked to discrepancies in the response to left and right rewards, we followed the next steps of analysis. First, for every neuron and every maze section, we calculated the mean value of the relative firing rate difference between left and right trials ($\widehat{D}_{start}(x)$, $\widehat{D}_{cue}(x)$, $\widehat{D}_{delay}(x)$, $\widehat{D}_{arms}(x)$, $\widehat{D}_{reward}(t)$). Then, for each neuronal group, we

calculated the linear relationship (Pearson's correlation) between the reward section mean values, to those in the remainder of the maze (Pearson's correlation; Figure 6C).

Immunohistochemistry

After completion of the recording sessions, which lasted about a month, mice were anesthetized with isoflurane and perfused transcardially with 10 ml PBS and 10 ml paraformaldehyde (4%), before they were decapitated. Brains were then removed, post-fixed and coronal slices (100 µm) were prepared. The primary antibodies used were rabbit anti-tyrosine hydroxylase (TH) and chicken anti-GFP. The secondary antibodies used were AlexaFluor 549 anti-rabbit and 488 IgG anti-chicken, respectively. Sections were further stained with DAPI to visualize nuclei. Image acquisition was performed with a fluorescence microscope NanoZoomer (Hamamatsu, Japan) system.

References

Goldman-Rakic, P.S., Leranth, C., Williams, S.M., Mons, N., and Geffard, M. (1989). Dopamine synaptic complex with pyramidal neurons in primate cerebral cortex. Proceedings of the National Academy of Sciences *86*, 9015-9019.

Ljungberg, T., Apicella, P., and Schultz, W. (1991). Responses of monkey midbrain dopamine neurons during delayed alternation performance. Brain research *567*, 337-341.

Sawaguchi, T., and Goldman-Rakic, P.S. (1991). D1 dopamine receptors in prefrontal cortex: involvement in working memory. Science *251*, 947-950.

Smiley, J.F., Williams, S.M., Szigeti, K., and Goldman‐Rakic, P.S. (1992). Light and electron microscopic characterization of dopamine‐immunoreactive axons in human cerebral cortex. Journal of Comparative Neurology *321*, 325-335.

Schultz, W., Apicella, P., and Ljungberg, T. (1993). Responses of monkey dopamine neurons to reward and conditioned stimuli during successive steps of learning a delayed response task. Journal of neuroscience *13*, 900-913.

Smiley, J.F., and Goldman-Rakic, P.S. (1993). Heterogeneous targets of dopamine synapses in monkey prefrontal cortex demonstrated by serial section electron microscopy: a laminar analysis using the silver-enhanced diaminobenzidine sulfide (SEDS) immunolabeling technique. Cerebral cortex *3*, 223-238.

Goldman-Rakic, P.S. (1995). Cellular basis of working memory. Neuron *14*, 477-485.

Goldman-Rakic, P.S. (1997). The cortical dopamine system: role in memory and cognition. Advances in pharmacology *42*, 707-711.

Schultz, W., Dayan, P., and Montague, P.R. (1997). A neural substrate of prediction and reward. Science *275*, 1593-1599.

Carr, D.B., and Sesack, S.R. (2000a). Projections from the rat prefrontal cortex to the ventral tegmental area: target specificity in the synaptic associations with mesoaccumbens and mesocortical neurons. Journal of neuroscience *20*, 3864-3873.

Carr, D.B., and Sesack, S.R. (2000b). GABA‐containing neurons in the rat ventral tegmental area project to the prefrontal cortex. Synapse *38*, 114-123.

Durstewitz, D., Seamans, J.K., and Sejnowski, T.J. (2000). Neurocomputational models of working memory. Nature neuroscience *3*, 1184-1191.

Floresco, S.B., and Phillips, A.G. (2001). Delay-dependent modulation of memory retrieval by infusion of a dopamine D_1 agonist into the rat medial prefrontal cortex. Behavioral neuroscience *115*, 934.

Miller, E.K., and Cohen, J.D. (2001). An integrative theory of prefrontal cortex function. Annual review of neuroscience *24*, 167-202.

Tzschentke, T.M. (2001). Pharmacology and behavioral pharmacology of the mesocortical dopamine system. Progress in neurobiology *63*, 241-320.

Cohen, J.D., Braver, T.S., and Brown, J.W. (2002). Computational perspectives on dopamine function in prefrontal cortex. Current opinion in neurobiology *12*, 223-229.

Dreher, J.-C., and Burnod, Y. (2002). An integrative theory of the phasic and tonic modes of dopamine modulation in the prefrontal cortex. Neural networks *15*, 583-602.

Schultz, W. (2002). Getting formal with dopamine and reward. Neuron *36*, 241-263.

Curtis, C.E., and D'Esposito, M. (2003). Persistent activity in the prefrontal cortex during working memory. Trends in cognitive sciences *7*, 415-423.

Montague, P.R., Hyman, S.E., and Cohen, J.D. (2004). Computational roles for dopamine in behavioural control. Nature *431*, 760-767.

820 Phillips, A.G., Ahn, S., and Floresco, S.B. (2004). Magnitude of dopamine release in
821 medial prefrontal cortex predicts accuracy of memory on a delayed response task.
822 Journal of Neuroscience *24*, 547-553.

823 Traub, R.D., Bibbig, A., LeBeau, F.E., Buhl, E.H., and Whittington, M.A. (2004).
824 Cellular mechanisms of neuronal population oscillations in the hippocampus in vitro.
825 Annu Rev Neurosci *27*, 247-278.

826 Wise, R.A. (2004). Dopamine, learning and motivation. Nature reviews neuroscience *5*,
827 483-494.

828 Fries, P. (2005). A mechanism for cognitive dynamics: neuronal communication
829 through neuronal coherence. Trends in cognitive sciences *9*, 474-480.

830 Tobler, P.N., Fiorillo, C.D., and Schultz, W. (2005). Adaptive coding of reward value
831 by dopamine neurons. Science *307*, 1642-1645.

832 Bäckman, C.M., Malik, N., Zhang, Y., Shan, L., Grinberg, A., Hoffer, B.J., Westphal,
833 H., and Tomac, A.C. (2006). Characterization of a mouse strain expressing Cre
834 recombinase from the 3′ untranslated region of the dopamine transporter locus.
835 genesis *44*, 383-390.

836 Buzsaki, G. (2006). Rhythms of the Brain (Oxford University Press).

837 Floresco, S.B., and Magyar, O. (2006). Mesocortical dopamine modulation of executive
838 functions: beyond working memory. Psychopharmacology *188*, 567-585.

839 Morris, G., Nevet, A., Arkadir, D., Vaadia, E., and Bergman, H. (2006). Midbrain
840 dopamine neurons encode decisions for future action. Nature neuroscience *9*, 1057-
841 1063.

842 Pierce, R.C., and Kumaresan, V. (2006). The mesolimbic dopamine system: the final
843 common pathway for the reinforcing effect of drugs of abuse? Neuroscience &
844 biobehavioral reviews *30*, 215-238.

845 Uhlhaas, P.J., and Singer, W. (2006). Neural synchrony in brain disorders: relevance for
846 cognitive dysfunctions and pathophysiology. neuron *52*, 155-168.

847 Berridge, K.C. (2007). The debate over dopamine's role in reward: the case for
848 incentive salience. Psychopharmacology *191*, 391-431.

849 Matsumoto, M., and Hikosaka, O. (2007). Lateral habenula as a source of negative
850 reward signals in dopamine neurons. Nature *447*, 1111-1115.

851 Vijayraghavan, S., Wang, M., Birnbaum, S.G., Williams, G.V., and Arnsten, A.F.
852 (2007). Inverted-U dopamine D1 receptor actions on prefrontal neurons engaged in
853 working memory. Nature neuroscience *10*, 376-384.

854 Fujisawa, S., Amarasingham, A., Harrison, M.T., and Buzsáki, G. (2008). Behavior-
855 dependent short-term assembly dynamics in the medial prefrontal cortex. Nature
856 neuroscience *11*, 823.

857 Lammel, S., Hetzel, A., Häckel, O., Jones, I., Liss, B., and Roeper, J. (2008). Unique
858 properties of mesoprefrontal neurons within a dual mesocorticolimbic dopamine
859 system. Neuron *57*, 760-773.

860 Nair-Roberts, R.G., Chatelain-Badie, S., Benson, E., White-Cooper, H., Bolam, J., and
861 Ungless, M. (2008). Stereological estimates of dopaminergic, GABAergic and
862 glutamatergic neurons in the ventral tegmental area, substantia nigra and retrorubral
863 field in the rat. Neuroscience *152*, 1024-1031.

864 Jhou, T.C., Geisler, S., Marinelli, M., Degarmo, B.A., and Zahm, D.S. (2009). The
865 mesopontine rostromedial tegmental nucleus: a structure targeted by the lateral habenula
866 that projects to the ventral tegmental area of Tsai and substantia nigra compacta. Journal
867 of Comparative Neurology *513*, 566-596.

868 Omelchenko, N., and Sesack, S.R. (2009). Ultrastructural analysis of local collaterals of
869 rat ventral tegmental area neurons: GABA phenotype and synapses onto dopamine and
870 GABA cells. Synapse *63*, 895-906.

871 Robbins, T.W., and Arnsten, A.F. (2009). The neuropsychopharmacology of fronto-
872 executive function: monoaminergic modulation. Annual review of neuroscience *32*,
873 267-287.

874 Tsai, H.-C., Zhang, F., Adamantidis, A., Stuber, G.D., Bonci, A., De Lecea, L., and
875 Deisseroth, K. (2009). Phasic firing in dopaminergic neurons is sufficient for behavioral
876 conditioning. Science *324*, 1080-1084.

877 Hauber, W. (2010). Dopamine release in the prefrontal cortex and striatum: temporal
878 and behavioural aspects. Pharmacopsychiatry *43*, S32-S41.

879 Fujisawa, S., and Buzsáki, G. (2011). A 4 Hz oscillation adaptively synchronizes
880 prefrontal, VTA, and hippocampal activities. Neuron *72*, 153-165.

881 Lammel, S., Ion, D.I., Roeper, J., and Malenka, R.C. (2011). Projection-specific
882 modulation of dopamine neuron synapses by aversive and rewarding stimuli. Neuron
883 *70*, 855-862.

884 Vong, L., Ye, C., Yang, Z., Choi, B., Chua Jr, S., and Lowell, B.B. (2011). Leptin
885 action on GABAergic neurons prevents obesity and reduces inhibitory tone to POMC
886 neurons. Neuron *71*, 142-154.

887 Buschman, T.J., Denovellis, E.L., Diogo, C., Bullock, D., and Miller, E.K. (2012).
888 Synchronous oscillatory neural ensembles for rules in the prefrontal cortex. Neuron *76*,
889 838-846.

890 Cohen, J.Y., Haesler, S., Vong, L., Lowell, B.B., and Uchida, N. (2012). Neuron-type-
891 specific signals for reward and punishment in the ventral tegmental area. nature *482*, 85-
892 88.

893 Harvey, C.D., Coen, P., and Tank, D.W. (2012). Choice-specific sequences in parietal
894 cortex during a virtual-navigation decision task. Nature *484*, 62-68.

895 Salamone, J.D., and Correa, M. (2012). The mysterious motivational functions of
896 mesolimbic dopamine. Neuron *76*, 470-485.

Stark, E., Koos, T., and Buzsáki, G. (2012). Diode probes for spatiotemporal optical control of multiple neurons in freely moving animals. Journal of neurophysiology *108*, 349-363.

Tan, K.R., Yvon, C., Turiault, M., Mirzabekov, J.J., Doehner, J., Labouèbe, G., Deisseroth, K., Tye, K.M., and Lüscher, C. (2012). GABA neurons of the VTA drive conditioned place aversion. Neuron *73*, 1173-1183.

van Zessen, R., Phillips, J.L., Budygin, E.A., and Stuber, G.D. (2012). Activation of VTA GABA neurons disrupts reward consumption. Neuron *73*, 1184-1194.

Howe, M.W., Tierney, P.L., Sandberg, S.G., Phillips, P.E., and Graybiel, A.M. (2013). Prolonged dopamine signalling in striatum signals proximity and value of distant rewards. nature *500*, 575-579.

Matsumoto, M., and Takada, M. (2013). Distinct representations of cognitive and motivational signals in midbrain dopamine neurons. Neuron *79*, 1011-1024.

Niv, Y. (2013). Dopamine ramps up. Nature *500*, 533-535.

Berényi, A., Somogyvári, Z., Nagy, A.J., Roux, L., Long, J.D., Fujisawa, S., Stark, E., Leonardo, A., Harris, T.D., and Buzsáki, G. (2014). Large-scale, high-density (up to 512 channels) recording of local circuits in behaving animals. Journal of neurophysiology *111*, 1132-1149.

Stokes, M.G. (2015). 'Activity-silent'working memory in prefrontal cortex: a dynamic coding framework. Trends in cognitive sciences *19*, 394-405.

Hamid, A.A., Pettibone, J.R., Mabrouk, O.S., Hetrick, V.L., Schmidt, R., Vander Weele, C.M., Kennedy, R.T., Aragona, B.J., and Berke, J.D. (2016). Mesolimbic dopamine signals the value of work. Nature neuroscience *19*, 117-126.

Berke, J.D. (2018). What does dopamine mean? Nature neuroscience *21*, 787-793.

Miller, E.K., Lundqvist, M., and Bastos, A.M. (2018). Working Memory 2.0. Neuron *100*, 463-475.

Engelhard, B., Finkelstein, J., Cox, J., Fleming, W., Jang, H.J., Ornelas, S., Koay, S.A., Thiberge, S.Y., Daw, N.D., and Tank, D.W. (2019). Specialized coding of sensory, motor and cognitive variables in VTA dopamine neurons. Nature *570*, 509-513.

Mohebi, A., Pettibone, J.R., Hamid, A.A., Wong, J.-M.T., Vinson, L.T., Patriarchi, T., Tian, L., Kennedy, R.T., and Berke, J.D. (2019). Dissociable dopamine dynamics for learning and motivation. Nature *570*, 65-70.

Ott, T., and Nieder, A. (2019). Dopamine and cognitive control in prefrontal cortex. Trends in cognitive sciences *23*, 213-234.

Choi, J.Y., Jang, H.J., Ornelas, S., Fleming, W.T., Fürth, D., Au, J., Bandi, A., Engel, E.A., and Witten, I.B. (2020). A comparison of dopaminergic and cholinergic populations reveals unique contributions of VTA dopamine neurons to short-term memory. Cell reports *33*, 108492.

Kim, H.R., Malik, A.N., Mikhael, J.G., Bech, P., Tsutsui-Kimura, I., Sun, F., Zhang, Y., Li, Y., Watabe-Uchida, M., and Gershman, S.J. (2020). A unified framework for dopamine signals across timescales. Cell *183*, 1600-1616. e1625.

Acknowledgments

This study was supported by the Ministry of Education, Culture, Sports, Science, and Technology (Grants-in-Aid for Scientific Research 18H02711 and 18H05525), the Mitsubishi Foundation, the Naito Foundation, and the Japan Agency for Medical Research and Development (AMED).

In memory of Miles Adrian Whittington. A true mentor and friend.

Author contributions

V.G. and S.F. designed the experiments. V.G. performed the experiments and analyzed the data. V.G. and S.F. wrote the paper.

Competing Interest Statements

The authors declare that they have no competing interests.

971 # Figure Titles and Legends

972

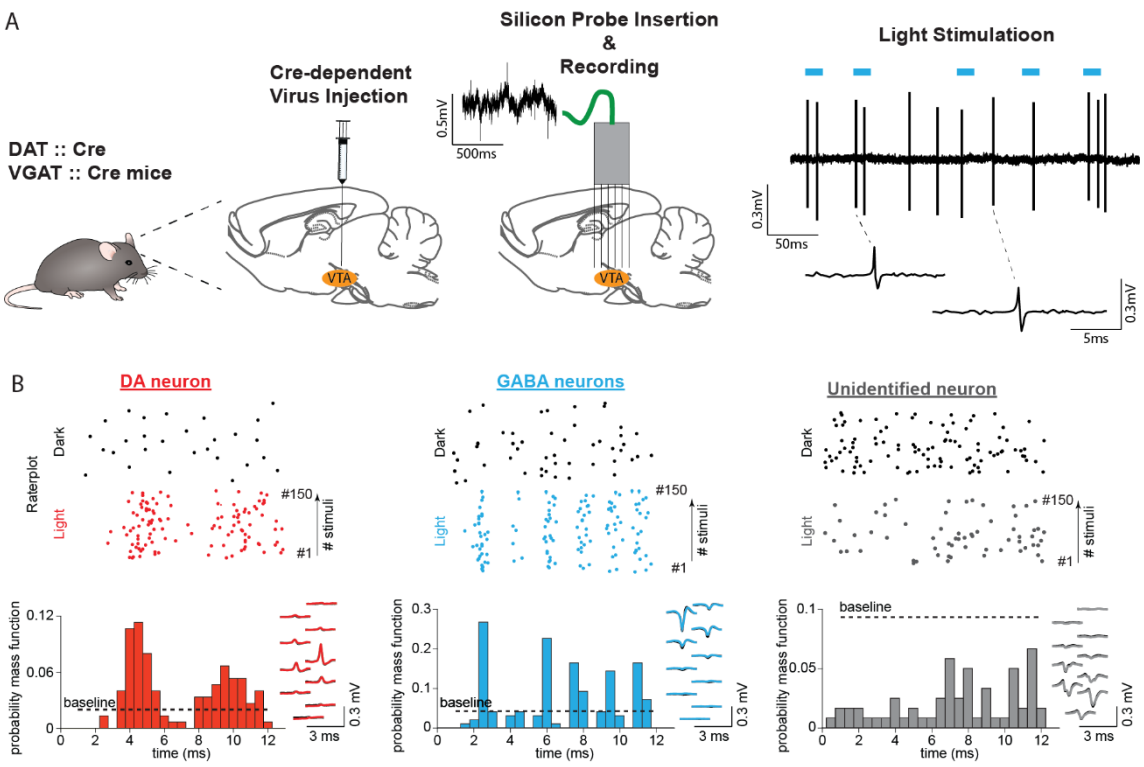

973 Fig 1

974 **Figure 1. Identifying midbrain dopaminergic and GABAergic neurons**

975 **(A)** Left: We confined ChR2 expression to DA and GABA neurons by injecting locally
976 into the VTA the adeno-associated virus FLEX-ChR2 into transgenic mice expressing
977 the Cre recombinase under the control of the promoter of the DA transporter
978 (DAT::Cre) or the vesicular GABA transporter (VGAT::Cre). Approximately 10 days
979 after the virus injection, the silicon probe was inserted into the brain in the same AP and
980 ML coordinates. On a daily basis, the probe was inserted deeper into the brain by a few
981 microns. Therefore, recording sessions were performed on different DV coordinates.

982 Right: High-pass filtered voltage trace recorded during a light-stimulation session.
983 Thick blue lines indicate light pulses (450 nm, 12 ms). Two light-induced spikes are
984 shown below.

(B) Light response patterns of representative DA (red), GABA (blue), and unidentified (gray) neurons. (Top) Raster plots of spikes discharged during light stimulation (colored dots) and in the inter-stimulus baseline period (baseline, black dots). (Bottom) PSTHs extracted from the light-induced spikes. The black dashed line indicates the upper confidence limit of the baseline activity. If it is exceeded by the light-induced PSTH, then the unit is identified as light-responsive (See Figure S2 for an explanation of this term). Right inset shows, superimposed, the mean waveforms of spontaneous (black) and light-induced (colored) spikes recorded by a single probe shank.

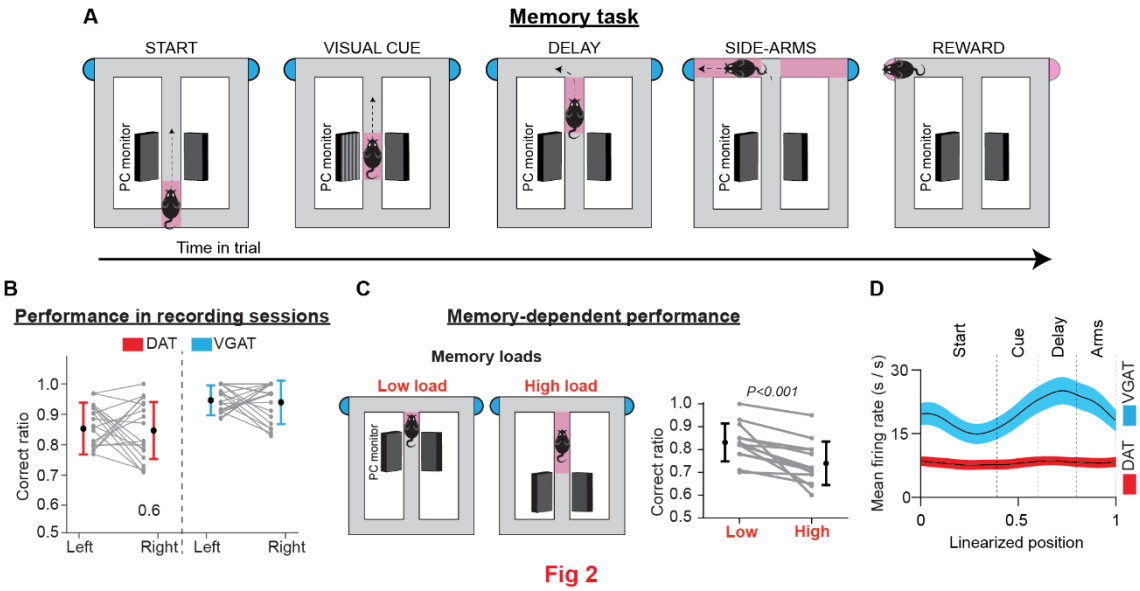

Figure 2. Memory task, performance and population activity.

(A) Schematic representation of the T-maze apparatus configuration in the memory task. Depending on the individual features of cognitive demand, the maze was divided into sections. Every trial commenced when the animal left the starting point, running along the central arm. In the visual cue section, a visual cue signaled the rewarded location. Between the visual cue section and the turning point at the end of the main arm, a brief memory delay was introduced. After reward consumption, the animals returned of their free will to the starting point to commence a new trial.

(B) Correct performance rates in sessions with electrophysiological recordings. Gray lines illustrate performance rates for left and right trials in every session. Colored lines illustrate performance averages across sessions (mean ± standard deviation) for DAT-Cre (red) and VGAT-Cre (blue) animals.

(C) In some training sessions animals received two blocks of trials with different memory loads. Gray lines illustrate correct performance rates for each block in every session and black lines show the average performance rates (mean ± standard deviation) across sessions, for all animals.

(D) Mean firing rates (thick lines) ± 1 standard error of the mean (shaded areas) of the population activities of DA (red) and GABA (blue) neurons. The averaged population firing activity of GABA neurons increased in the cue and delay sections. However, the averaged population activity of DA neurons did not deviate from the beginning until the end of the trials.

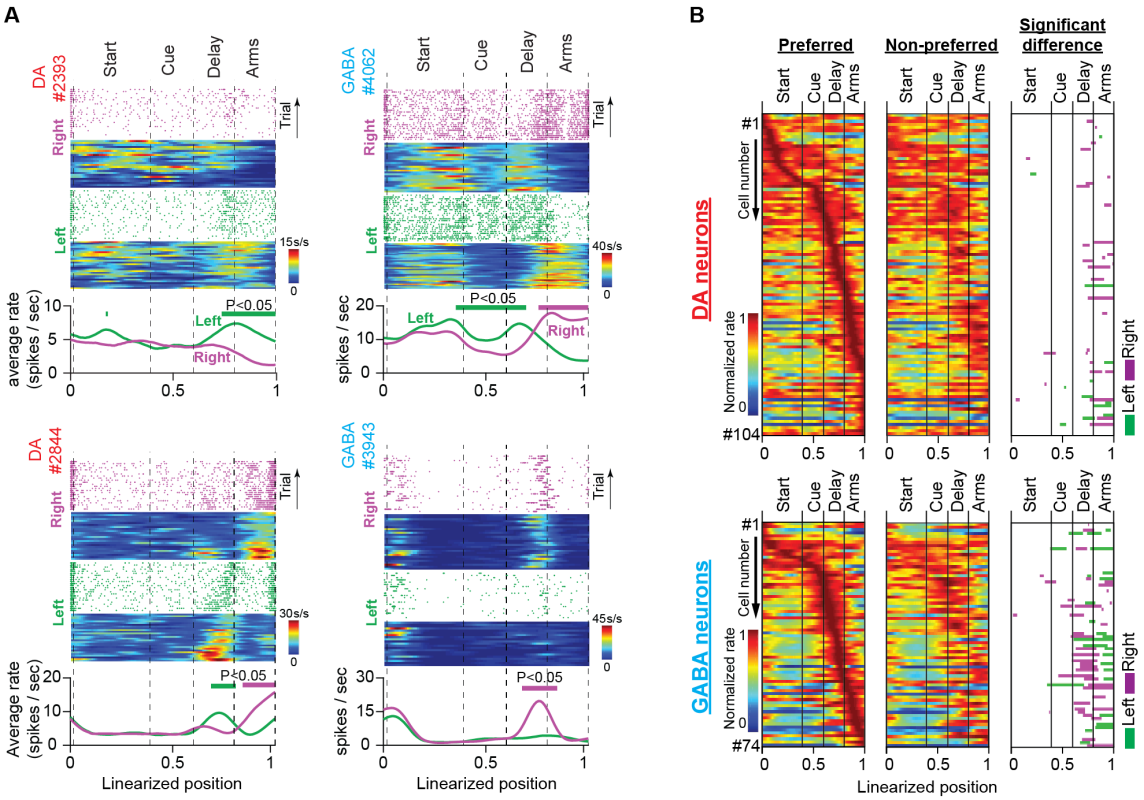

Fig 3

Figure 3. Trajectory-specific activities by DA and GABA neurons in the memory task

(A) Firing patterns of representative DA and GABA neurons. In each example: (Top) Raster plots of spiking events, for every correct trial, and their corresponding firing rate heatmaps as a function of position during right (purple) and left (green) trials. (Bottom) Average firing rates for correct left and right trials. Note that the trial and average firing rates (spikes/sec) are plotted as a function of position but normalized by the amount of time the mouse occupied each position on every trial. Thick lines above the average firing rates represent segments with significantly different firing rates between right and left correct trials (See also Figure S4; permutation test; $P < 0.05$). It is evident in these examples that midbrain neurons differentiate their discharge rates between left and right trajectories in certain positions.

(B) Heatmaps of neuronal population responses organized by preferred lap trajectory (i.e., the trajectory with the stronger response; first column) and non-preferred lap

trajectory (i.e., the trajectory with the weaker response; second column) for DA neurons (Top; n = 104 units, 35 sessions in five mice) and GABA neurons (Bottom; n = 74 units, 25 sessions in four mice). Each row contains preferred and non-preferred trajectory responses of the same neuron. In every row, both responses are normalized by the maximum rate of the preferred trajectory. The third column shows maze segments with significantly different discharge rates between preferred and non-preferred trajectories.

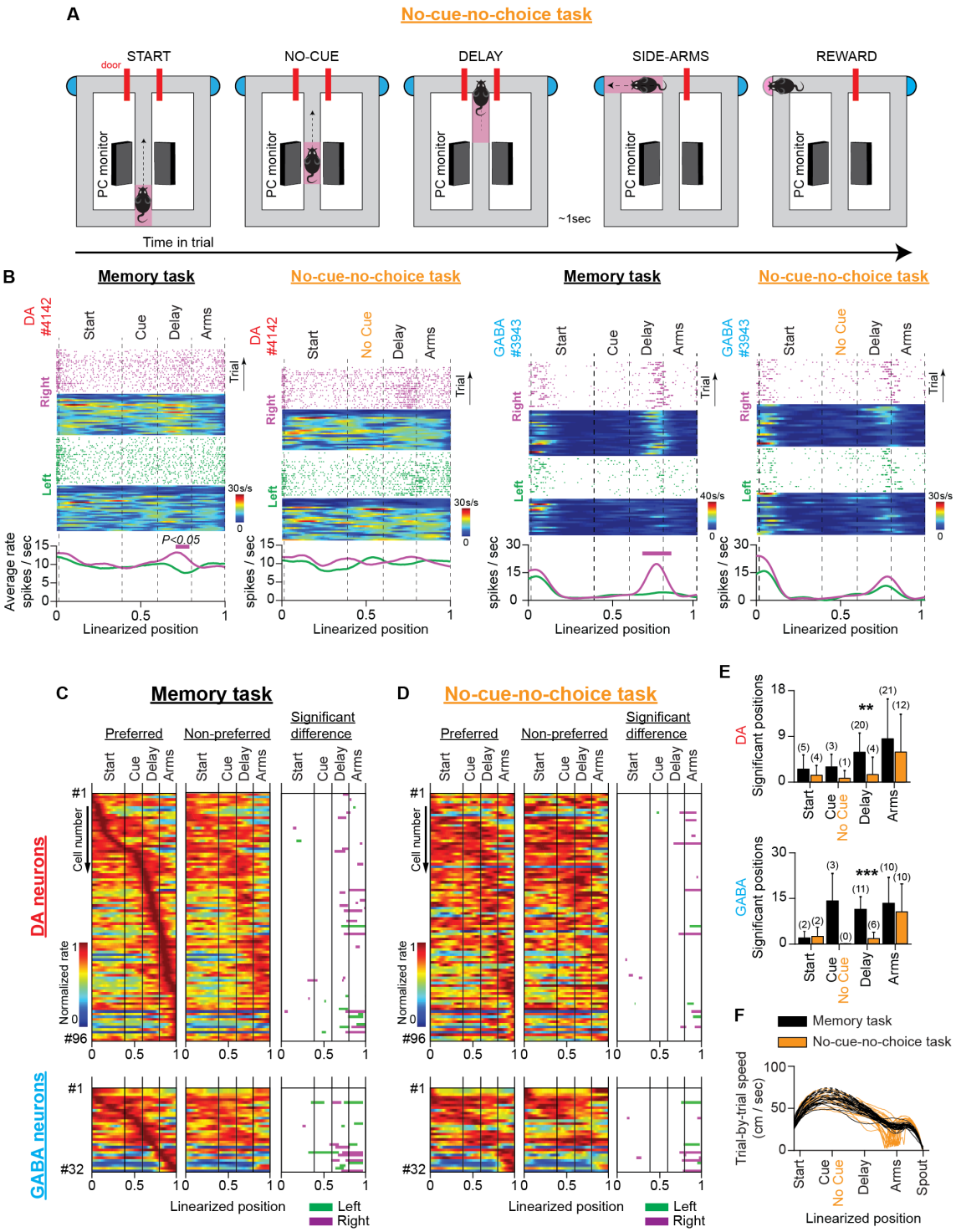

Fig 4

Figure 4. VTA neuronal responses in a T-maze task without visual cues and memory-dependent decisions (no-cue-no-choice task)

(A) Schematic representation of the T-maze apparatus illustrating the sequence of events in the no-cue-no-choice task.

(B) Firing patterns of representative DA (left) and GABA (right) neurons during the memory and no-cue-no-choice tasks. Both examples illustrate that the trajectory-specific firing rate difference in the delay section of the memory task declines prominently in the control task when animals do not receive visual cues which indicates the reward location, or make memory-dependent decisions.

(C and D) The firing patterns of DA neurons (C; $n = 96$ units, 30 sessions in four mice) and GABA neurons (D; $n = 32$ units, 12 sessions in three mice) in the memory task and the no-cue-no-choice task recorded in the same sessions. (Left and Middle columns) Normalized average neuronal responses for preferred (left) and non-preferred (middle) trajectories. The right column represents the maze segments with significantly different discharge rates. The row order of the neurons is the same for the memory task and the control task heatmaps. The data shown here for the memory task are a subset of those shown in Figure 3B.

(E) Average number of position points (mean ± standard deviation) with a significant rate difference, arranged by maze section and behavioral task for DA (left) and GABA (right) neurons (** $P < 0.01$, *** $P < 0.001$, paired *t*-test comparing numbers of significant position points between tasks. Also, the numbers in parentheses describe the number of neurons with a significant rate difference).

(F) Representative example showing the prominent difference in running speeds (cm/s) between the memory (black) and no-cue-no-choice (brown) task trials in a single session.

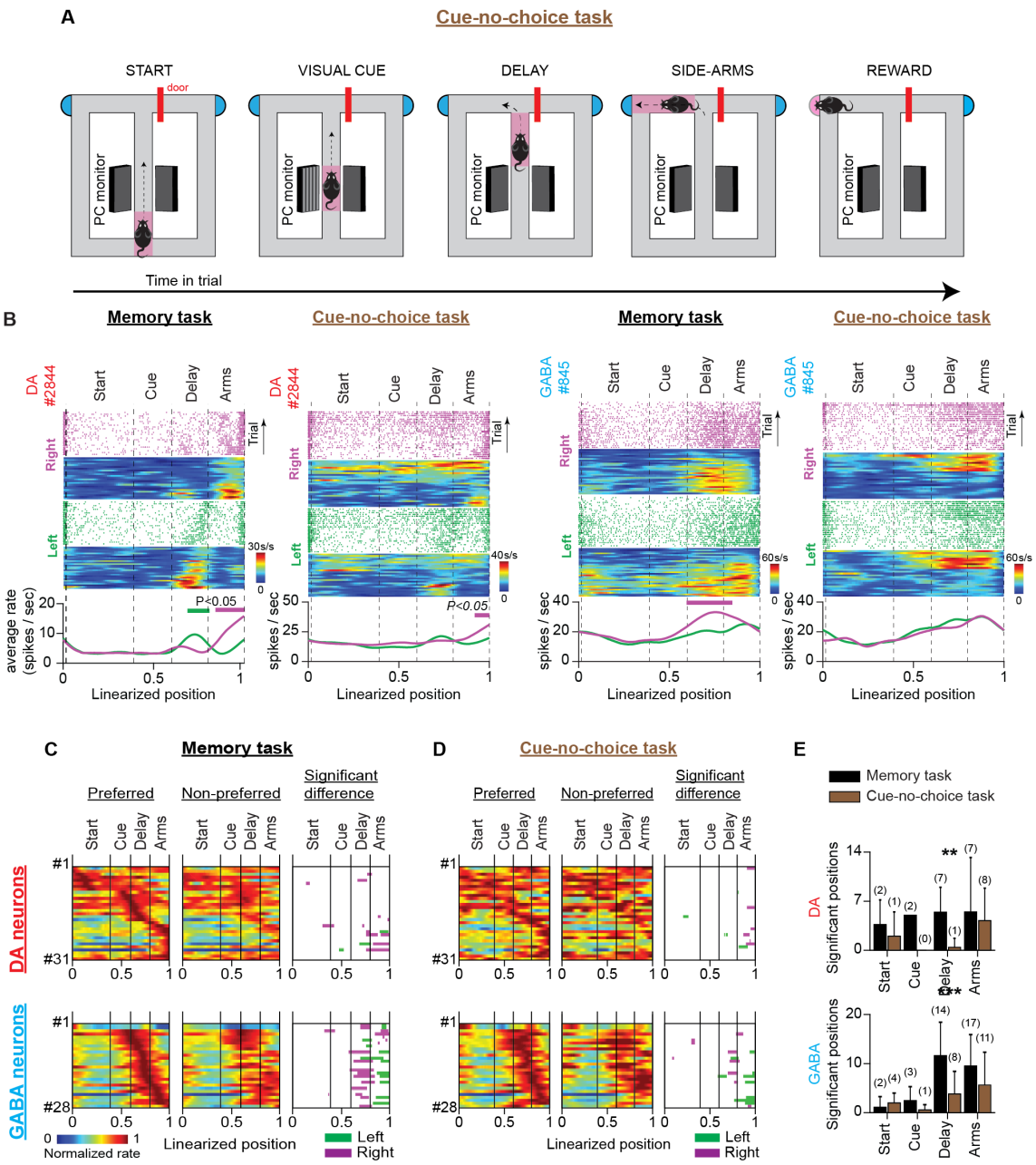

Fig 5

Figure 5. VTA neuronal responses in a T-maze task with visual cues but no memory-dependent decisions (cue-no-choice task)

(A) Schematic representation of the T-maze apparatus illustrating the sequence of events in the cue-no-choice task.

1086 **(B)** Firing patterns of representative DA (left) and GABA (right) neurons during the
1087 memory and cue-no-choice tasks. Both examples illustrate that the trajectory-specific
1088 firing rate difference in the delay section of the memory task becomes notably weaker in
1089 the cue-no-choice task when animals do not make memory-dependent decisions,
1090 although running speed activities and incentive motivational drives of physical effort
1091 are the same between tasks.

1092 **(C and D)** The firing patterns of DA neurons (C; n = 31 units, 28 sessions in four mice)
1093 and GABA neurons (D; n = 28 units, 11 sessions in one mouse) in the memory task and
1094 the cue-no-choice task recorded during the same sessions. (Left and Middle columns)
1095 Normalized average neuronal firing rates associated with the preferred (left) and non-
1096 preferred (middle) trajectories. The right column represents the maze segments with
1097 significantly different discharge rates. The row order of the neurons is the same for the
1098 memory task and the control task heatmaps. The data shown here for the memory task
1099 are a subset of those shown in Figure 3B.

1100 **(E)** Average number of position points (mean ± standard deviation) with significant rate
1101 differences, arranged by maze section and behavioral task for (left) DA and (right)
1102 GABA neurons (** $P < 0.01$, *** $P < 0.001$, paired t-test comparing numbers of
1103 significant position points between tasks. Also, the numbers in parentheses describe the
1104 number of neurons with a significant rate difference).

1105

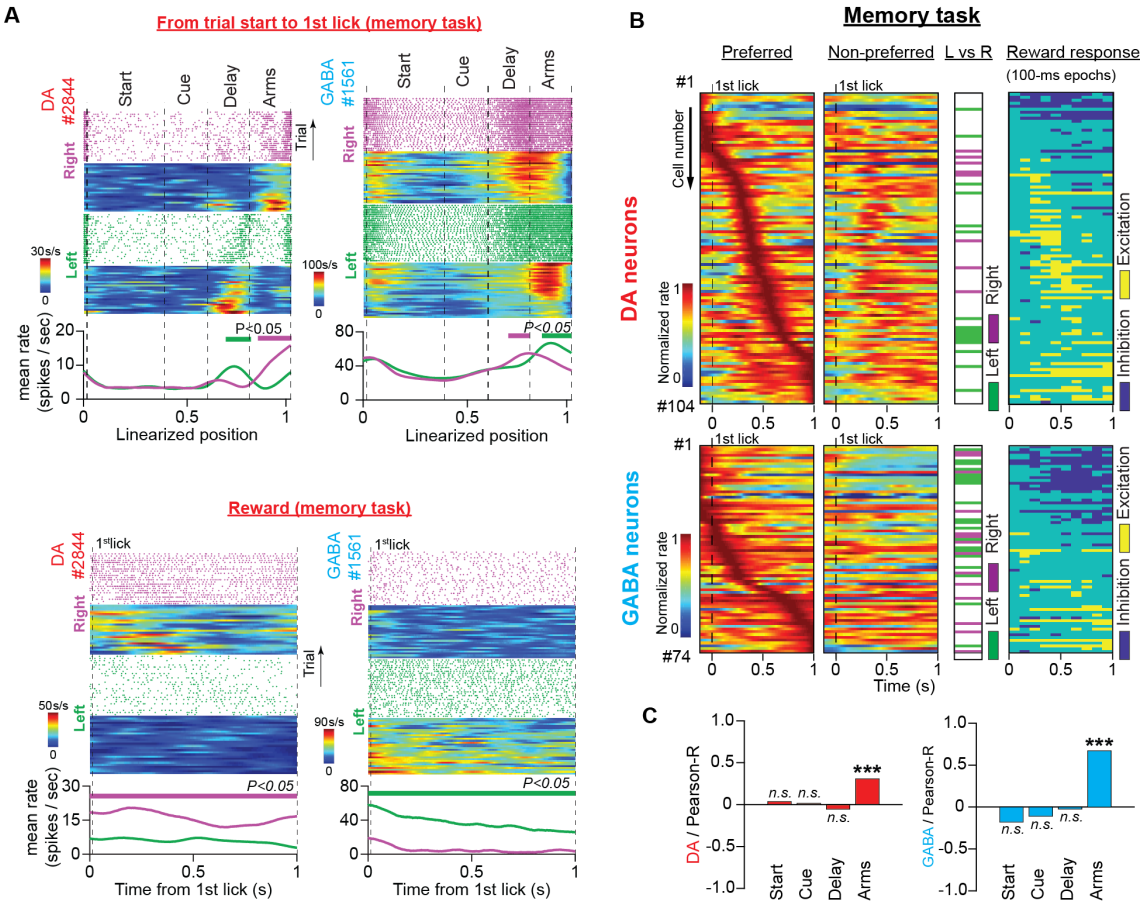

Fig 6

Figure 6. Neuronal responses during reward consumption are not related to the trajectory-specific activities in the memory delay

(A) Firing patterns of representative DA and GABA neurons in the memory task for the period from trial start until the first lick of the waterspout, which triggered the water pump (top, space domain) and during reward consumption (bottom, time domain).

In each example: (Top) Raster plots of the spike trains and their corresponding firing rate heatmaps arranged by trajectory and position (maze) or time (reward) in right (purple) and left (green) trials. (Bottom) Average firing rates for correct left and right trials. The thick lines above the firing rates represent segments with significantly different firing rates between the correct right and left trials.

(B) Firing patterns of DA (top) and GABA (bottom) neurons in the time domain during reward consumption (from the first lick until 1 s later) for preferred (first column) and

1119 non-preferred (second column) rewards (DA: n = 104 units, 35 sessions in five mice;
1120 GABA: n = 74 units, 25 sessions in four mice). Each row represents the normalized
1121 average firing rates (preferred and non-preferred) of a single neuron on a color scale.
1122 Neurons were ordered according to the time point of the maximum rate in the preferred
1123 arm. The third column shows neurons with significant discrepancies between the left
1124 and right reward-related responses (paired t-test for mean firing rates, $P < 0.05$). The
1125 fourth column shows post-delivery reward segments (100 ms each) with significant
1126 excitation or inhibition compared with the 100-ms pre-reward segment (paired t-test
1127 comparing firing rates, $P < 0.05$).

1128 **(C)** Correlations between the mean firing rate difference in the reward section and the
1129 difference in every other maze section for DA (left) and GABA (right) neurons
1130 (Pearson's R values with P-values, *** $P < 0.001$). Only the trajectory-specific firing
1131 rate difference in the side arms correlated with the reward-specific rate difference.

1132

1133

1134

1135

1136

1137

1138

1139

1140

1141

Supplementary Materials for

Memory-specific encoding activities of the ventral tegmental area dopamine and GABA neurons

Vasileios Glykos[1], Shigeyoshi Fujisawa[1]*

Correspondence to: shigeyoshi.fujisawa@riken.jp

This PDF file includes:

- Supplementary Text 1
- Figs 1–8
- Table 1

Supplementary Texts:

Supplementary Text 1. Evaluating the contribution of behavioral variables in trajectory-specific activity with multiple regression analysis

We designed a generalized linear regression model in which the dependent variable was the position-arranged firing rate, and the independent variables (predictors) were the animal's running speed, trial number, performance rate (cumulative correct rate), current trial accuracy (reward or not), previous trial accuracy (reward history), and lap trajectory (left or right). Since the permutation analysis of the original spike trains revealed that the trajectory-specific effect on neuronal firing activity was highly dependent on the animal's position (occurring mainly in the delay and side-arm sections), we included the joint effect of lap trajectory and position in the training model instead of testing the effect of trajectory alone. A major advantage of regression analysis is that one can dissociate the inherently bound effects of the independent variables. For

example, we can examine the influence of the lap trajectory variable on neuronal firing activity without including the effect of the running speed variable (which could potentially differ between left and right trials).

For each neuron, we produced model predictions for the correct left and right trial average firing rates (Figure. S6A, dashed lines) from which we calculated the predicted firing rate difference. We subsequently examined the contribution of each independent variable to the trajectory-specific firing activity by shuffling the trajectory labels assigned only to this particular variable. If the tested variable exerts a significant effect on the firing rate, then shuffling the trajectory labels would produce a significant reduction in the predicted firing rate difference. We examined the same pool of neurons that we reported on the memory task, as shown in Figure 3B (n=104 DA and n=74 GABA-identified neurons). In the delay region, the joint effect of lap trajectory and position (trajectory × position predictor) contributed significantly to the predicted average rate difference of 23 DA neurons (Figure S6B and S6C top), 17 of which overlapped with the 22 trajectory-specific neurons identified with the permutation analysis (Figure S6C bottom). Of the GABA neurons, 34 were modulated by trajectory and position (Figure S6B and S6C top), 30 of which were also trajectory-specific (Figure S6C bottom). These results confirm that the trajectory factor was responsible for the firing rate difference shown in Figure 3B. The speed variable significantly modulated 24 DA and 22 GABA neurons (Figure S6B and S6C top), but only four DA and four GABA neurons were co-modulated by trajectory (Figure S6C bottom). The performance and accuracy variables modulated smaller numbers of neurons (Figure S6B and S6C top), and the reward outcome of the previous trial did not co-modulate any of the trajectory-specific DA and GABA neurons (Figure S6C bottom). The trial variable modulated 30 DA neurons and 32 GABA neurons, co-modulating with the trajectory variable of 8 DA and 15 GABA neurons. However, the distribution of the trial predictor coefficient did not differ from a distribution with a mean equal to zero (one-sample *t*-test, $P > 0.05$, Figure S6D), indicating that the effect of successive trials on firing rate did not reflect cognitive processing, but was caused by mechanical reasons; due to the animal's movements, the distance of the recording channel from the targeted neurons changed continuously, which affected the signal-to-noise ratio and eventually spike

detection. In agreement with Engelhard et al., a notable proportion of DA neurons (36%) and GABA neurons (74%) were co-modulated by more than one behavioral variable Figure S6E (Engelhard et al., 2019).

Overall, the regression analysis confirmed the results of the permutation analysis regarding the significant effect of trajectory on midbrain neuronal activity during memory-dependent decisions. In addition, it demonstrated that the remaining independent variables included in our model cannot fully explain trajectory-specific firing activities in the delay period of the memory task.

1219 **Supplementary Figures:**

1220

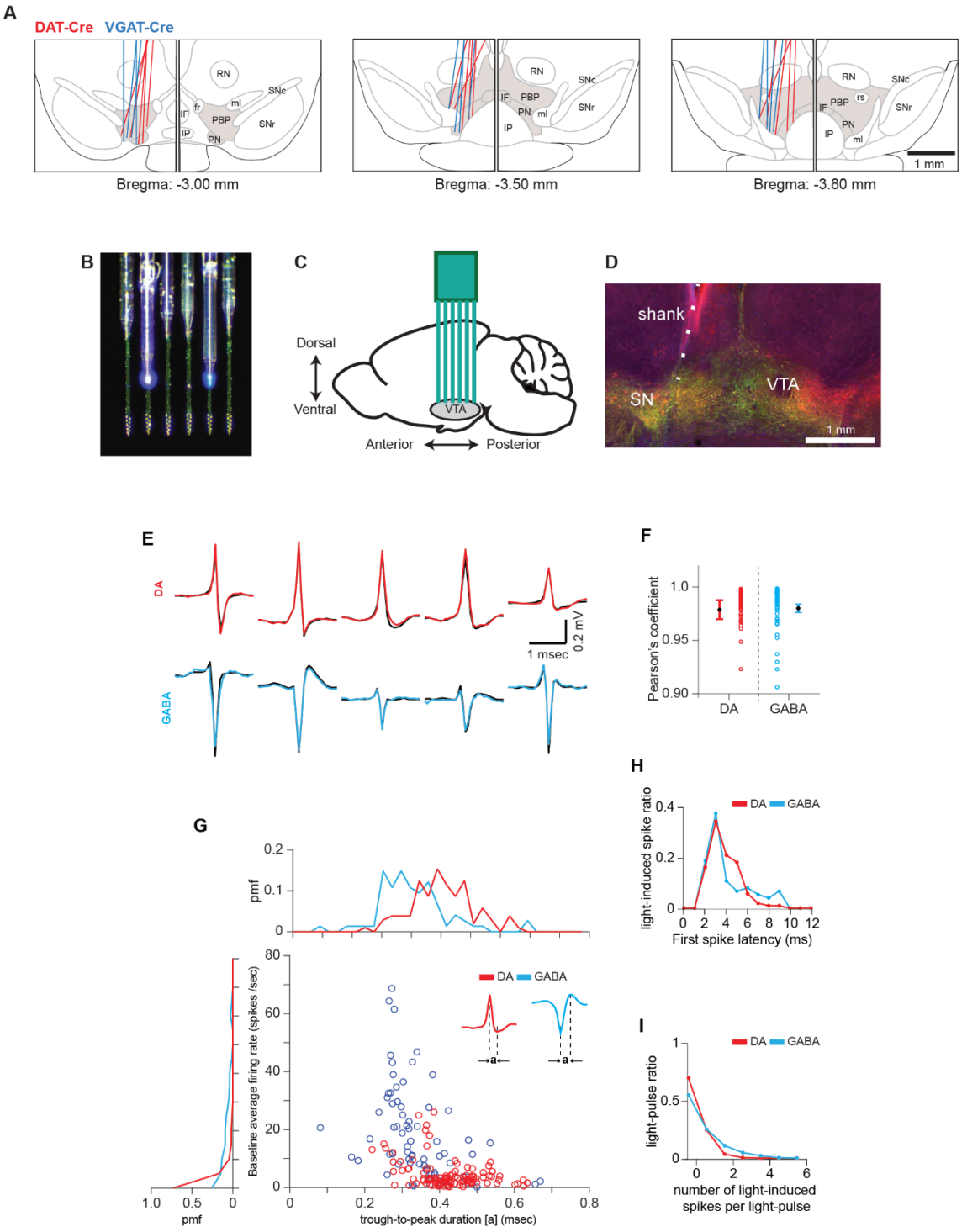

Fig S1

1221

1222 **Figure S1. Validation of optogenetic identification results. Related to Figure 1.**

1223 **(A)** Serial reconstructions of recording sites along the rostro-caudal axis of coronal
1224 midbrain slices for DAT-Cre (red) and VGAT-Cre (blue) animals. *fr*: fasciculus
1225 retroflexus, IF: interfascicular nucleus, IP: interpeduncular nucleus, *ml*: medial
1226 lemniscus, PBP: parabrachial pigmented nucleus, PN: paranigral nucleus, RN: red
1227 nucleus, *rs*: rubrospinal tract, SNc: substantia nigra pars compacta, SNr: substantia
1228 nigra pars reticulata.

1229 **(B)** Photograph of the silicon probe with attached optical fibers. Optical fibers (core
1230 diameter 50 μm) were glued to the shanks to ensure a firm, accurate, and durable
1231 insertion into the deep midbrain. Optical fibers on shanks 2 and 5 were coupled to blue
1232 laser diodes (450 nm), maintaining a certain distance from the tip of the shank to ensure
1233 that blue light could irradiate the whole span of the recording electrode array.

1234 **(C)** Schematic drawing of the mouse brain in the sagittal plane, illustrating the insertion
1235 of the silicon probe into the VTA.

1236 **(D)** Immunofluorescence microscopy image of a coronal brain slice of a DAT-Cre
1237 mouse injected with the optogenetic virus in the left VTA. DAT: dopamine transporter
1238 (red); YFP: yellow fluorescent protein (green); SN: substantia nigra. NOTE: the white
1239 dashed line highlights the trace by the probe shank on the tissue.

1240 **(E)** Mean waveforms of light-induced (colored) and spontaneous (black) spikes
1241 discharged by identified DA (red) and GABA (blue) neurons in a single light
1242 stimulation session.

1243 **(F)** Pearson's correlation coefficient between the waveforms of spontaneous and light-
1244 induced spikes for the identified DA (red) and GABA (blue) neurons. The light-induced
1245 spike waveforms were almost identical to the spontaneous waveforms for all the
1246 identified neurons. This was reflected by the high mean correlation coefficient (mean ±
1247 standard error of the mean; DA: $r = 0.98 \pm 0.09$, $P < 0.05$; GABA: $r = 0.98 \pm 0.03$, $P <$
1248 0.05).

1249 **(G)** Trough-to-peak spike duration vs. average spontaneous firing rate raster plot for the
1250 identified DA (red) and GABA (blue) neurons. The side plots show the distributions of
1251 the X- and Y-axis values in the main plot (pmf: probability mass function). In
1252 agreement with earlier reports (2) DA neurons fired spikes with lower rates (DA: 4.50 ±
1253 5.00 spikes/sec, GABA: 17.34 ± 15.72 spikes/sec; unpaired t-test comparing the
1254 spontaneous rates: $t_{(176)} = 7.80$, $P < 0.001$) and wider waveforms (DA: 0.46 ± 0.08 ms,
1255 GABA: 0.34 ± 0.10 ms; unpaired t-test comparing trough-to-peak values: $t_{(176)} = 5.96$, P
1256 < 0.001) than the GABA neurons.

1257 **(H)** Latency of the first spike discharged during light stimulation for the identified DA
1258 (red) and GABA (blue) neurons.

1259 **(I)** Number of light-induced spikes per light pulse for DA (red) and GABA (blue)
1260 neurons.

1261

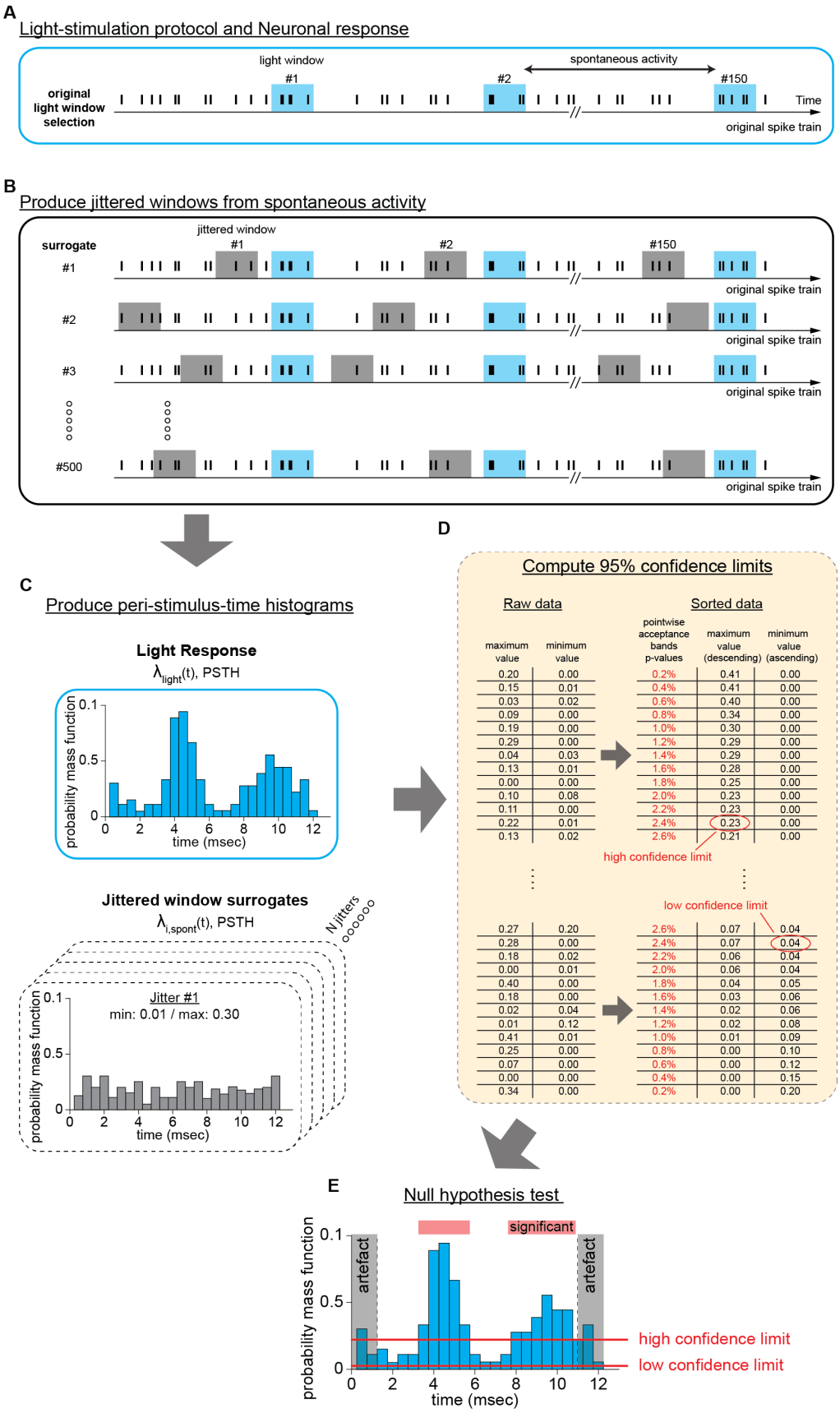
A
Light-stimulation protocol and Neuronal response
light window
spontaneous activity
#1
#2
#150
original light window selection
Time
original spike train
B
Produce jittered windows from spontaneous activity
jittered window
surrogate
#1
#2
#3
#500
original spike train
C
Produce peri-stimulus-time histograms
Light Response
λlight(t), PSTH
probability mass function
time (msec)
Jittered window surrogates
λi,spont(t), PSTH
N jitters
Jitter #1
min: 0.01 / max: 0.30
D
Compute 95% confidence limits
Raw data
Sorted data
maximum value
minimum value
pointwise acceptance bands p-values
maximum value (descending)
minimum value (ascending)
high confidence limit
low confidence limit
E
Null hypothesis test
significant
artefact
high confidence limit
low confidence limit

Fig S2

1263 **Figure S2. Statistical method for optogenetic identification. Related to Figure 1.**

1264 To identify the light-responsive units, we compared the light-induced average responses
1265 to average spontaneous firing activity. To this end, we used the following jittering
1266 method.

1267 **(A)** Schematic representation of a spike train during a light stimulation session. Vertical
1268 black bars represent spiking events. The blue shaded areas indicate the light-stimulation
1269 windows. The firing activity between light stimulations is spontaneous.

1270 **(B)** To identify light-responsive units we raised the hypothesis that the relative firing
1271 rate during light stimulation, $\hat{\lambda}_{light}(t)$, did not differ from the spontaneous firing rate,
1272 $\hat{\lambda}_{spont}(t)$. To do so, we employed a jittering method in which a randomly jittered
1273 window (12 ms) fitted in the spontaneous activity period preceding the light-pulse (that
1274 is, the jittered window onset never preceded the offset of the preceding light-pulse and
1275 the offset never succeeded the onset of the succeeding light pulse). We produced as
1276 many jittered windows as the light-pulses and we repeated this process 500 times in
1277 total.

1278 **(C)** For every neuron we produced peri-stimulus-time-histograms (PSTHs, 12 ms, 1 ms
1279 bins) of the relative firing rate, by superimposing the spike trains of every light
1280 stimulation pulse. If $n^{(k)}(t)$ is the number of spikes of a single neuron in post-light
1281 onset time t of the k_{th} stimulation pulse, then, the average firing rate, $\hat{\lambda}(t) = \frac{1}{K} * \frac{1}{T} *$
1282 $\sum_{k=1}^{K} n^{(k)}(t - t_0)$, where K is the number of stimulation pulses, T is the bin size (1 ms)
1283 and t_0 the light-pulse onset time, represents the relative firing rate at time t . In the end
1284 we produced one $\hat{\lambda}_{light}(t)$ and 500 $\hat{\lambda}_{spont}(t)$ firing rates.

1285 **(D)** From every, $\hat{\lambda}_{i,spont}(t)$ histogram we extracted the maximum and minimum values
1286 and stored them in two separate vectors. Vectors were sorted, and from them, the 95%
1287 confidence limits were calculated. These were the 2.5% largest value from the
1288 maximum PSTH vector and the 2.5% smallest value from the minimum PSTH vector

(that is 13rd from the 500 rows). Units with $\hat{\lambda}_{light}(t)$ PSTH exceeding at any time point (between 1 ms and 11ms) the high confidence limit, were identified as light-responsive.

(E) If the $\hat{\lambda}_{light}(t)$ PSTH fell below the low confidence limit at any time point, then the unit was characterized as light-inhibited due to synaptic transmission (we did not find any light-inhibited units). Otherwise, those units whose PSTH did not violate any of the confidence limits were characterized as unidentified.

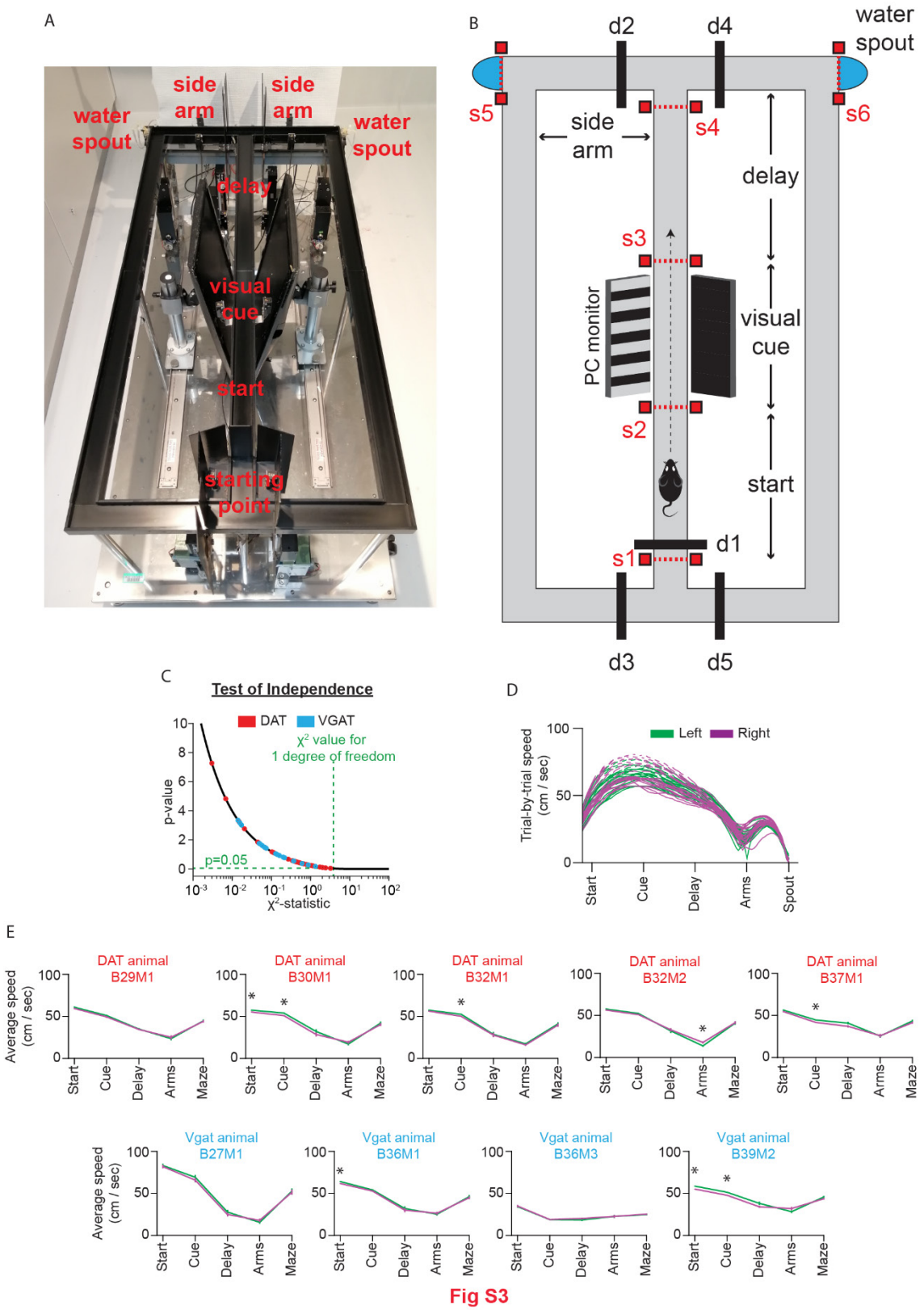
A
side arm
side arm
water spout
water spout
delay
visual cue
start
starting point
B
d2
d4
water spout
s5
s6
side arm
s4
delay
s3
PC monitor
visual cue
s2
start
d1
s1
d3
d5
C
Test of Independence
DAT
VGAT
χ² value for 1 degree of freedom
p-value
p=0.05
χ²-statistic
D
Left
Right
Trial-by-trial speed (cm / sec)
Start
Cue
Delay
Arms
Spout
E
DAT animal B29M1
DAT animal B30M1
DAT animal B32M1
DAT animal B32M2
DAT animal B37M1
Average speed (cm / sec)
Start
Cue
Delay
Arms
Maze
Vgat animal B27M1
Vgat animal B36M1
Vgat animal B36M3
Vgat animal B39M2

Fig S3

1296

Figure S3. T-maze configuration, behavior and running speed assessment in the memory task. Related to Figure 2.

(A) Photograph of the T-maze apparatus with maze sections labeled. The mice were trained on different variations of an associative T-maze task with visual instruction cues. The behavioural apparatus was a Figure-eight T-maze (O'Hara & CO., LTD, Tokyo, Japan), 50 cm tall, with a main arm (120 cm) and side arms (30 cm each). Infrared light-beam sensors placed at key position points on the maze defined the beginning and end of the successive maze sections. The apparatus was equipped with sliding doors, which prevented the animals from developing unwanted behavior (e.g. moving backwards). Sensor activations were on-line monitored, and significant behavioural events (e.g. visual-cue presentation, reward delivery, door opening/closing) were dictated by an in-house behavioural software written in MATLAB (Mathworks, MA, USA), through a multi-signal processor interface system (RX6; Tucker-Davis Technologies, FL, USA). The moment-by-moment position of the animal on the maze apparatus was monitored continuously by a video tracking system, composed of a red light-emitting diode mounted on the mouse head stage and a video camera (39 frames/sec) hung by the room ceiling. Video data were stored for offline analysis.

(B) Detailed schematic representation of the T-maze apparatus. Infrared light-beam sensors (s1–s6) were mounted securely at key positions on the maze to define the beginning and end of the maze sections (start: s1–s2; visual cue: s2–s3; delay: s3–s4; side-arms: s4–s5/s6; reward: s5/s6). The first activation of s5 or s6 sensors (i.e., 1st lick) triggered the water-delivery pump. Five sliding doors restrained the animals from unwanted moves. Every trial began with the animal activating s1. At this point, the doors d1, d3, and d5 remained closed, isolating the animal in the starting location for approximately 2 s. This served two purposes: (1) to drain the waterspouts and (2) to prevent the animal from making decisions on the next trial guided by the previous trial outcome. After door d1 opened, the animal could run freely along the main arm. Activating s2 and s3 resulted in the visual cue onset and offset, respectively. Activating s5 triggered the left water-delivery pump, and door d3 opened while d1 closed. Activating s6 triggered the right water-delivery pump, and door d5 opened while d1

closed. In the memory task, doors d2 and d4 were always open. In the no-cue-no-choice task, doors d2 and d4 were initially closed. However, when the mouse activated s4, one door opened pseudo-randomly.

(C) To assess the influence of behavioural left-right biasing in decision making we applied the chi square (χ^2) test of independence. The null hypothesis was that correct performance was independent of behavioural choices. Black line illustrates the chi-squared distribution for 1 degree of freedom, along with the χ^2 values from the independence test for every session (DAT-Cre: red dots and VGAT-Cre: blue dots). The test was passed in every session (the level of significance was set to 5%, corresponding to $\chi^2 = 3.84$ for 1 degree of freedom).

(D) Representative example of trial speeds (cm/sec) in a single recording session of the memory task.

(E) Shown are running speeds (mean ± standard error of the mean) categorized by maze sections and averaged across sessions for left (green) and right (magenta) trials for individual VGAT-Cre and DAT-Cre mice. Although differences were small, they occasionally reached significance. Importantly, we did not detect speed differences between left and right trials in the delay section (unpaired t-test between left and right speed per region, * $P < 0.05$).

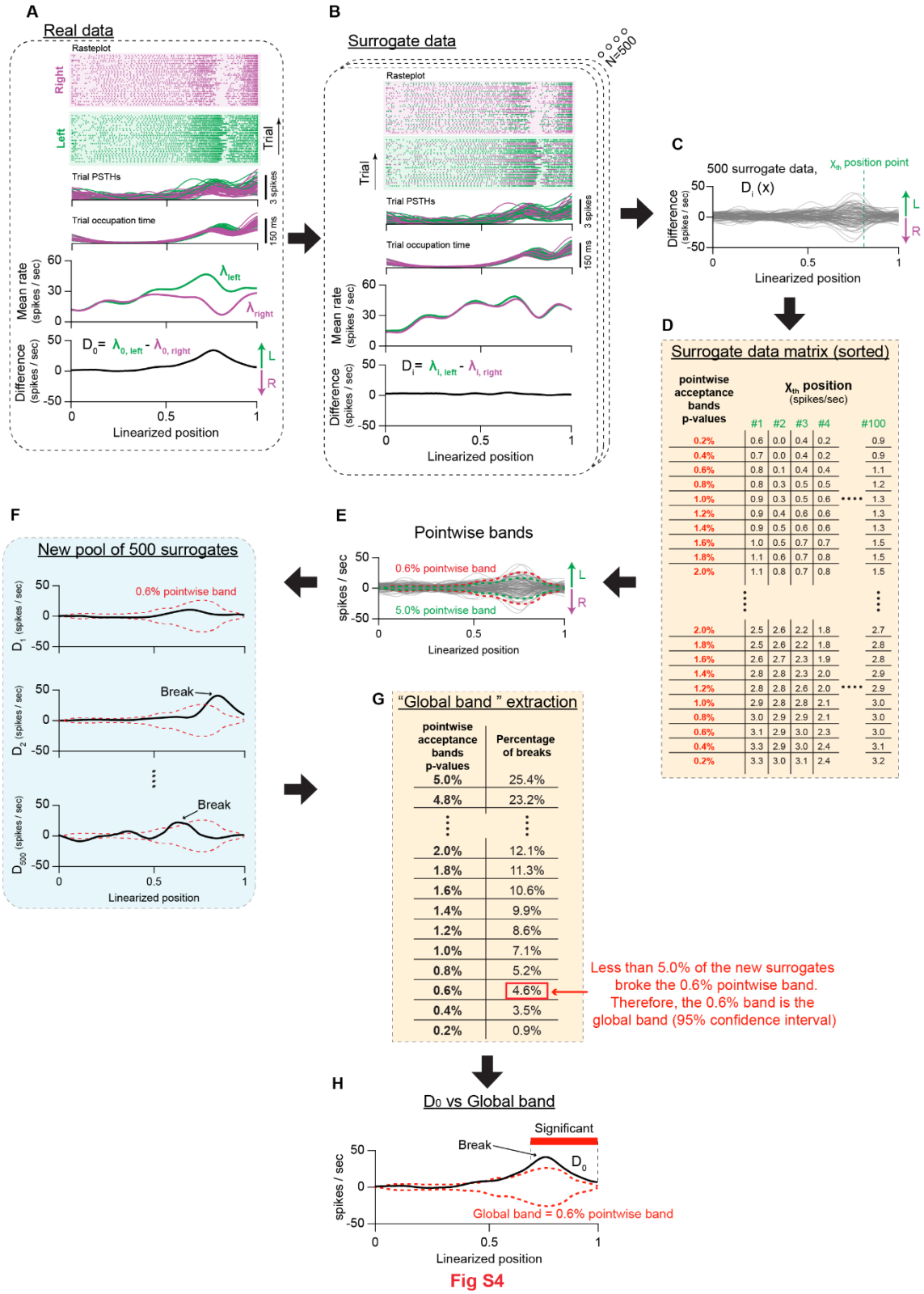

1346

1347 **Figure S4. Statistical method for identifying trajectory-specific neurons**

1348 **(permutation method). Related to Figure 3.**

We applied a permutation method reported elsewhere (Fujisawa et al., 2008) to identify neurons with trajectory-specific encoding properties. The motivation behind this analysis is that if the lap trajectory contributes to the firing rate difference observed at certain positions, then shuffling the trajectory labels assigned to the spike trains of individual trials would cause a marked reduction in the rate difference. This process is described below.

(A) From the spike trains of the correct left and right trials (top; raster plot), we estimated the trial relative firing rates ($\hat{\lambda}_{Left}(x)$ and $\hat{\lambda}_{Right}(x)$; middle). Importantly, we considered the variability in occupation time between positions and trials. Hence, to calculate the firing rates, we divided the number of spikes occurring in every position and trial (trial PSTHs) by the occupation time in the same position and for the same trial (trial occupation time). We subsequently produced the original average rate difference ($D_0(x)$, bottom) between the left- and right-correct trials.

(B) We shuffled the trajectory labels assigned to the trial spike trains along with the respective occupation times and re-calculated the difference $D_i(x)$ of the permuted labels.

(C) We produced 500 surrogates with permuted differences $D_i(x)$. In the end, we created a 500-by-100 matrix (shuffles-by-position) of $D_i(x)$ surrogates.

(D, E) From these surrogates we extracted the 95% confidence interval (lower and upper confidence limits) for the null hypothesis test. To do so, first, we calculated the confidence interval of each position point x. The difference values $D_i(x)$ in every position (column) were sorted and every row in the new matrix was treated as a potential confidence limit with different *P*-value. We term it as "pointwise acceptance band". If the original data $D_0(x)$ breaks the pointwise band, it corresponds to rejecting the null hypothesis at position x. However, if this procedure is repeated for every position x (i.e., 100 position points) in the maze, it raises the issue of multiple comparisons.

(F, G) To address this, we constructed the "global band", which can control errors of any false rejection across multiple indices. We produced another 500 permutations and calculated the percentage of the surrogate data $D_j(x)$ that broke the pointwise band candidates at any position points. If the percentage was more than 5%, we replaced the pointwise band with lower P-value. We repeated this process until a pointwise band candidate was exceeded by less than 5% of the new surrogates. When this happened, the pointwise band was used as the "global band" (i.e., 95% confidence interval) for the hypothesis test.

(H) The null hypothesis was rejected if the original difference $D_0(x)$, exceeded at any position x the global band. Then, the spatial extent of significance was defined by the number of position points exceeding the 95% confidence interval.

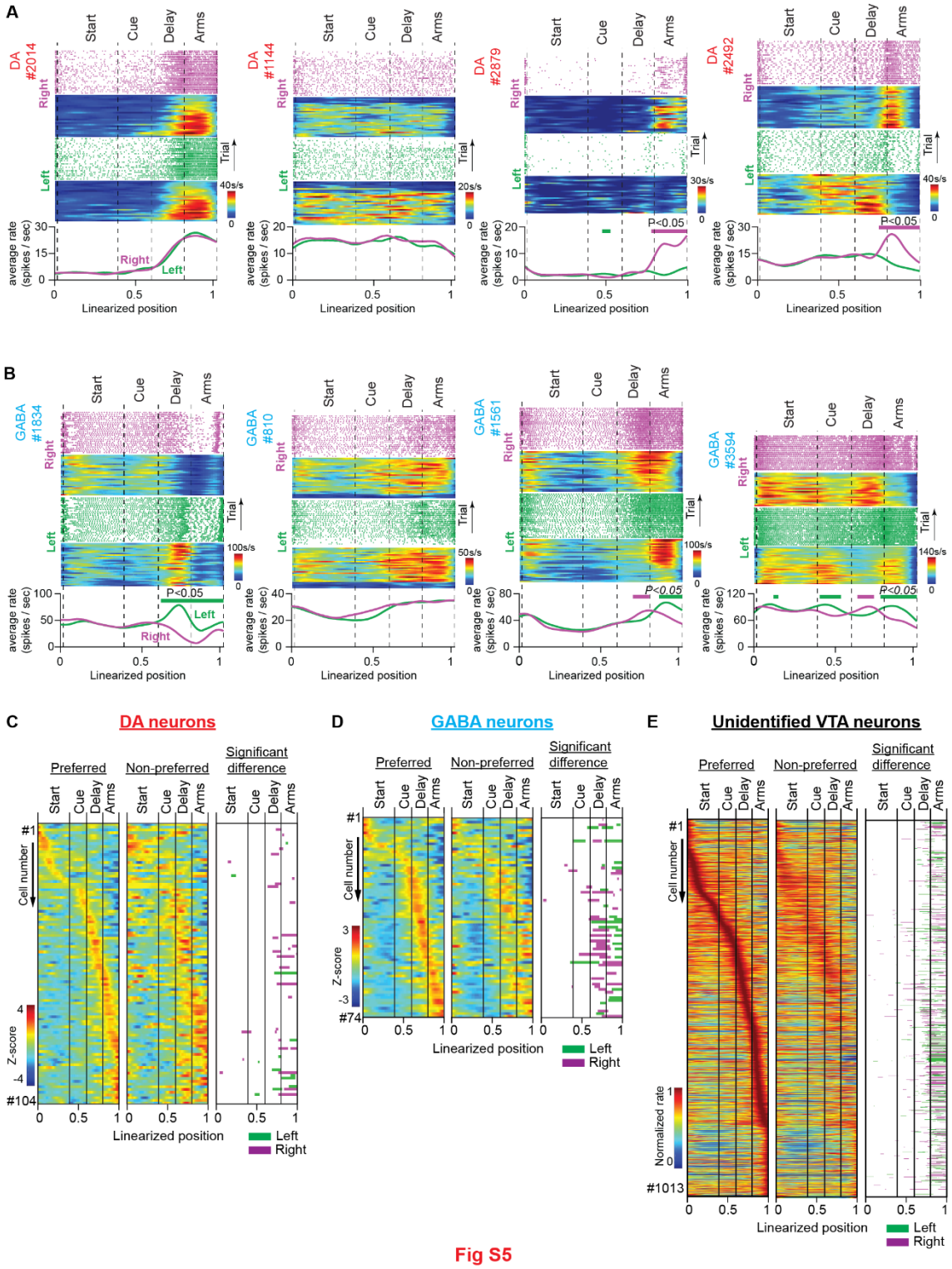

Fig S5

Figure S5. Firing activities of midbrain DA and GABA neurons in the memory task. Related to Figure 3.

All plots included in this figure were obtained from data recorded in the memory task.

(A and B) Representative discharge activity of DA (a) and GABA (b) neurons. In each example: (Top) Raster plots of the spikes, arranged by trial, and their corresponding firing rate heatmaps as a function of position in right (purple) and left (green) trials. (Bottom) Average firing rates for correct left and right trials. Note that the firing rate (spikes/s) is plotted as a function of position but has been normalized by the amount of time the mouse occupied each position in every trial. The thick lines above the firing rates represent segments with significantly different firing rates between the correct right and left trials.

(C and D) Heatmaps of the standardized average firing rates for the preferred (first column) and non-preferred (second column) trajectories of DA (c) and GABA (d) neurons. These plots show the number of standard deviations by which the average firing rate varied above or below the mean rate of correct trials as a function of the position on the maze. The row arrangement was the same as that in Figure 3B. The third column of the significant firing-rate difference is the same as that in the third column in Figure 3B.

(E) Heatmaps of the normalized average firing rate for preferred (first column) and non-preferred (second column) trajectories and the significant difference between them (third column) for the unidentified VTA neurons.

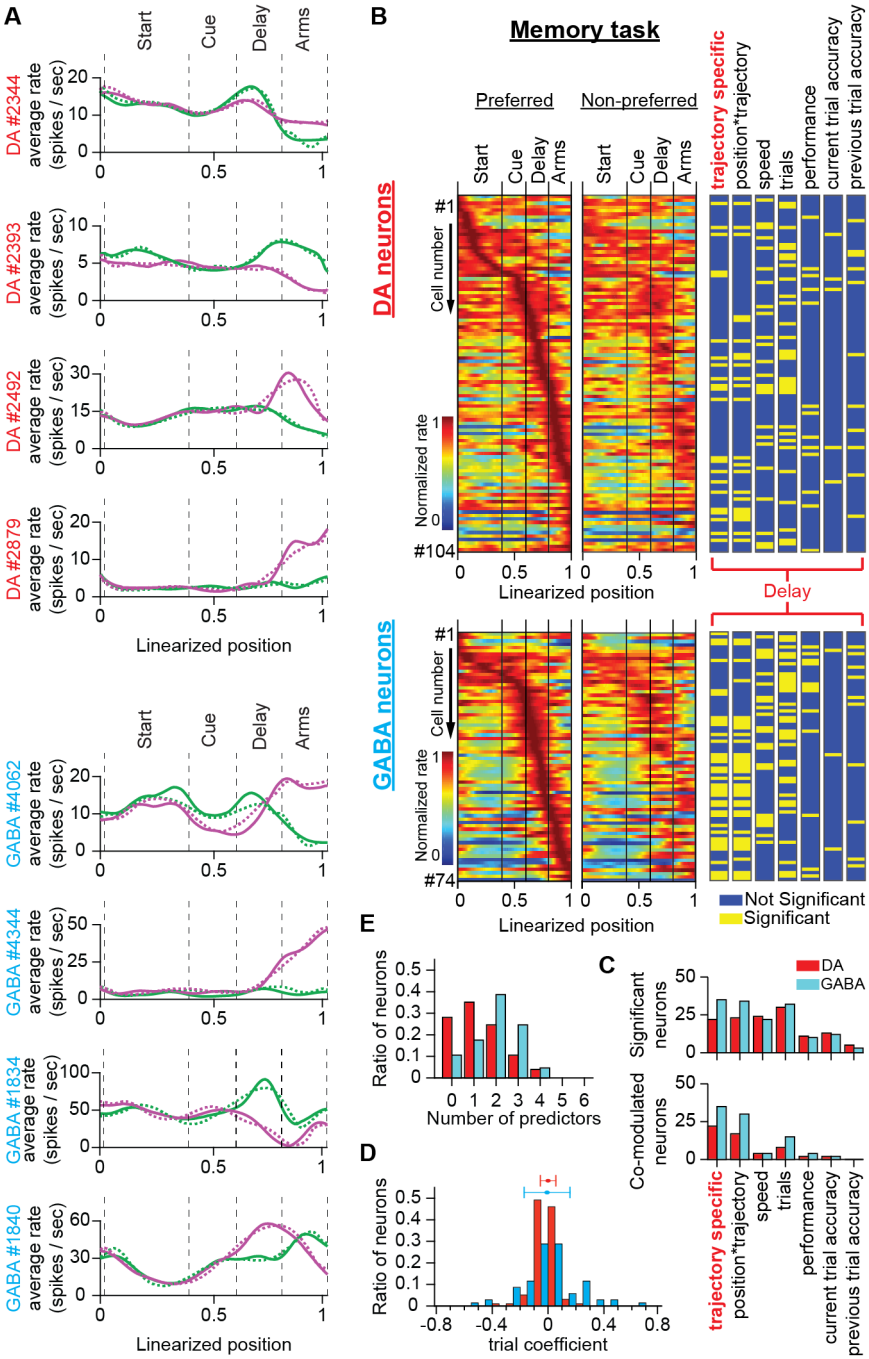

Fig S6

Figure S6. Evaluating DA and GABA neuronal responses to specific behavioral variables in the memory task through regression analysis. Related to Figure 3.

(A) Average firing rates of representative DA and GABA neurons extracted from real firing rate data (solid lines) and encoding model predictions (dashed lines) for left (green) and right (magenta) trials.

(B) (Left and Middle columns) Normalized firing rate heatmaps for preferred and non-preferred trajectories for DA and GABA neurons recorded in the memory task (the same as the ones in Figure 3B). (Right column) Significant contributions in the firing rate difference (yellow lines) by individual behavioral variables in the memory delay extracted with the permutation analysis of the encoding model predictions.

(C) (Top) Number of neurons significantly modulated by one of the independent variables. (Bottom) Number of neurons co-modulated by trajectory (trajectory-specific) and one of the individual variables. (Note: In B and C, the trajectory-specific neurons correspond to the significant neurons extracted using the permutation analysis of the original firing rates; third column in Figure 3B).

(D) The distribution of the trial coefficient for DA and GABA neurons along with the mean ± standard deviation values.

(E) Histogram of the number of independent behavioral variables co-modulating neurons in the delay region.

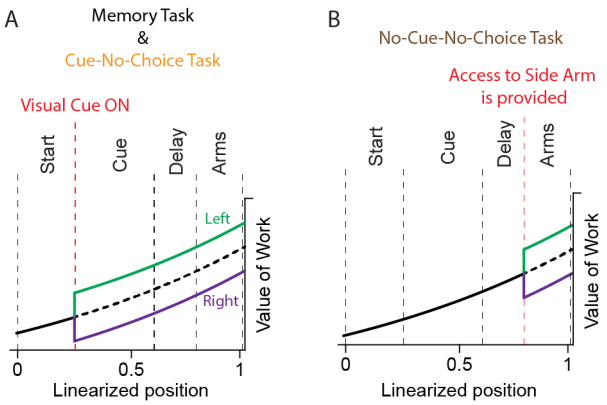

Fig S7

Figure S7. The dopamine signaling model of incentive motivational drive. Related to Figures 2, 3 and 4.

Striatal DA levels ramp up when mice navigate a maze or corridor in search for reward (Howe et al., 2013; Hamid et al., 2016; Kim et al., 2020). Initially, this evidence challenged theoretical neuroscientists, since the time-course of this ramping activity (lasting a few seconds) did not conform either with the prediction-error (RPE, phasic activity) or reward rate (tonic activity) theories (Niv, 2013). However, further research on this topic, provided empirical evidence to support a theory that DA conveys a signal for incentive motivational drive in the form of state-action value (value of work; (Hamid et al., 2016), or its derivative RPE; (Kim et al., 2020)).

Accordingly, the motivational value of future rewards is exponentially discounted with time or distance (the theory was developed on an adaptive decision-making framework; Hence the value of reward is defined by reward probability; figure 4 in (Hamid et al., 2016)). Different reward values correspond to different functions of discounted state-action values. If a cue predicts a reward with higher value, then the state-action value jumps to the discounted value function of that reward.

In our study, key parameters that could potentially influence incentive motivational drives were equal between left and right trials (reward amount, lap trajectory distance, etc.) and moreover, behavioral performance did not indicate choice biasing (Figures S3C). However, we cannot rule out the possibility that left and right rewards were valued differently, producing distinct value functions. If this is true, then the trajectory-

specific activities elicited by subgroups of DA and GABA neurons could reflect differences in the state-action values for left and right trials, and not memory-dependent decisions.

(A) The plot illustrates the hypothesis of different discounted value functions (i.e., the state-action value is a function of position and trajectory). In the memory task and the cue-no-choice task the assignment of the state-action value function takes place when the visual cue signals which reward is available.

(B) However, in the no-cue-no-choice task, the assignment occurs only when the mice are given access to one of the side arms.

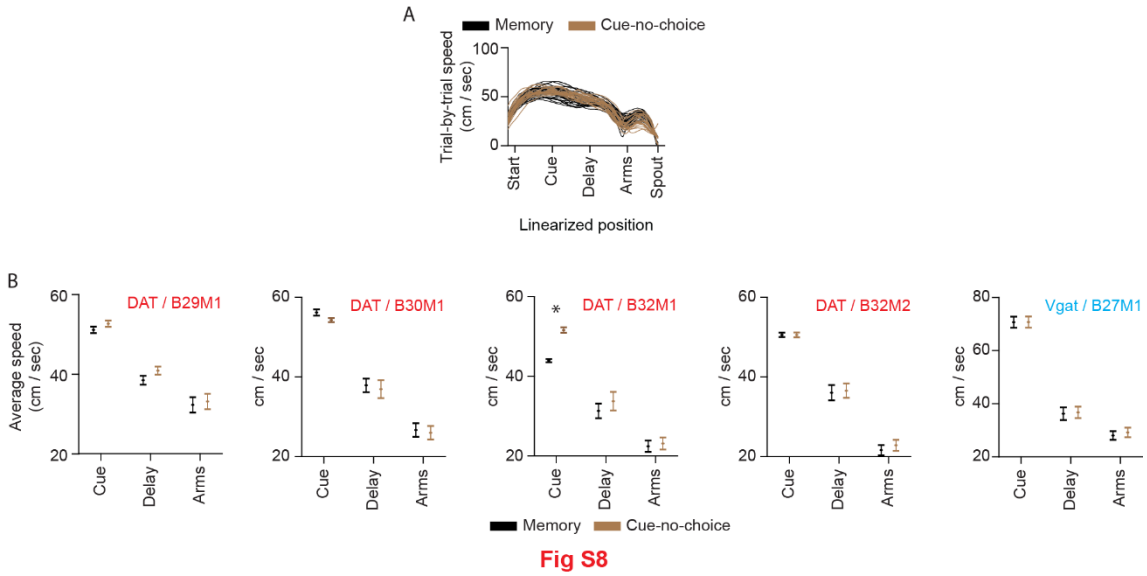

Figure S8. Running speed differences between the memory task and the cue-no-choice task. Related to Figures 3 and 5

(A) Representative example of running speeds (cm/s) for memory (black) and cue-no-choice (orange) trials in a single session. Speed differences were evident at the T-intersection (between delay and arms).

(B) Average running speed values (mean ± standard error of the mean) grouped by maze section and behavioral task for each of the DAT-Cre and VGAT-Cre animals performing the memory and cue-no-choice tasks. Importantly, no differences were detected in the delay and side-arm sections between memory (black) and cue-no-choice (brown) task trials (* $P < 0.05$, unpaired t-test on speed).

1490 **Supplementary Table:**
1491

1492 **Table S1. Number of neurons with trajectory-specific firing activities in the**
1493 **memory task grouped by maze section**

1494 Data are presented for all recorded neurons and individually for optogenetically
1495 identified DA and GABA neurons; DA, dopamine; GABA, gamma-aminobutyric acid.

Memory task: Significant difference in firing rate between left and right trials					
	start	cue	delay	side arms	reward
All (*n* = 1,191)	*n* = 49 (4%)	*n* = 78 (7%)	*n* = 377 (32%)	*n* = 505 (42%)	*n* = 461 (39%)
DA (*n* = 104)	*n* = 4 (4%)	*n* = 3 (3%)	*n* = 22 (21%)	*n* = 23 (22%)	*n* = 24 (23%)
GABA (*n* = 74)	*n* = 4 (5%)	*n* = 11 (15%)	*n* = 35 (47%)	*n* = 35 (47%)	*n* = 34 (46%)

1496

1497

1498 **SI References**

1499 *All references have been already cited in the main manuscript*

1500

1501

1502